

# 1           **Geometry and Kinematics of Salt-detached Ramp Syncline Basins**

2           \*Leonardo M. Pichel<sup>1</sup>; Frank Peel<sup>2,3</sup>, Christopher A-L. Jackson<sup>2,3</sup>; Mads Huuse<sup>1</sup>,

3

4           1 – School of Earth and Environmental Sciences, University of Manchester, Oxford  
5           Road, Manchester M13 9PL, UK

6           2 – The University of Texas at Austin, Bureau of Economic Geology, Jackson  
7           School of Geosciences, Austin, Texas, USA

8           3 – Basins Research Group (BRG), Department of Earth Science and Engineering,  
9           Imperial College London, South Kensington Campus, SW7 2BP, United Kingdom

10

11          Corresponding author: [leonardo.munizpichel@manchester.ac.uk](mailto:leonardo.munizpichel@manchester.ac.uk)

12          +44 (0) 7479011308

13          [Frank.peel@beg.utexas.edu](mailto:Frank.peel@beg.utexas.edu)

14          [C.jackson@imperial.ac.uk](mailto:C.jackson@imperial.ac.uk)

15          Mads.huuse@manchester.ac.uk

16

17

18          Key-words: SALT TECTONICS, RAMP-SYNCLINE BASINS, MINIBASINS,  
19          TRANSLATION, BASE-SALT RELIEF, GRAVITY-DRIVEN DEFORMATION

20

21

22

23

24

25

## Highlights

- Ramp syncline basins were identified above thick salt in the São Paulo Plateau, Santos Basin
- They form by translation over a thick salt detachment with basal relief due to viscous drag and salt flux variations
- They record 28-32 km of SE translation during the Late Cretaceous to Paleocene
- They form by translation over basinward-dipping and landward-dipping base-salt ramps
- Stratal terminations and architecture vary along-dip and strike within these systems

26

## ABSTRACT

27 Ramp-syncline basins (RSBs) are characterized by asymmetric depocentres  
28 formed by translation above salt detachments with basal steps. 3D seismic data  
29 from the São Paulo Plateau, Santos Basin, Brazil, image a series of RSBs formed  
30 above thick salt and distributed above and/or basinward of the main base-salt  
31 steps in the area. The RSBs are composed of landward-dipping and gently folded  
32 sigmoidal strata, recording 28-32 km of SE-oriented translation during the Late  
33 Cretaceous and Paleocene, at an average rate of 0.8-0.9 mm/year. We present  
34 examples of RSBs in the area and numerical forward models in order to analyse  
35 their 3D kinematics and interaction with base-salt structures. The RSBs form not  
36 only by translation above basinward-dipping ramps but also over landward-dipping  
37 ramps. Translation over stepped ramps generates stacked RSBs. Thickness maps  
38 show translation is higher at the centre of RSBs and that depocentres become  
39 progressively more affected by diapirism as the system evolves. Stratal  
40 architecture and terminations vary along dip and strike in these systems. This  
41 study presents the first ever analysis of the 3D kinematics of ramp-syncline basins,  
42 and the first documentation of their occurrence above thick salt in the Santos  
43 Basin, Brazil. It applies more realistic models that treat the detachment as a  
44 volume of viscous material, improving our understanding of these systems. Their  
45 recognition allows quantification of overburden translation above a deforming salt  
46 layer and the identification of basement topography, thus aiding the understanding  
47 and exploration of salt basins.

48

49

50

51

52

53

54 **1. Introduction**

55 Ramp-syncline basins (RSBs) are common features in extensional basins, being  
56 first recognized in the Gulf of Lyon, offshore France (e.g. Benedicto et al. 1999;  
57 Sanchis and Séranne, 2000) and the Kvamshesten Basin, onshore Norway  
58 (Osmundsen et al. 2000). They were initially described through conceptual (Gibbs,  
59 1984) and physical models (Ellis and McClay, 1988; McClay, 1990, 1996; McClay  
60 and Scott, 1991), as being formed above the hangingwall of ramp-flat extensional  
61 faults whose basal detachments dip in the direction of tectonic transport. The  
62 hanging wall is warped down above the ramp to create a local basin. As the  
63 hangingwall block moves, the locus of subsidence (located above the footwall  
64 ramp) remains fixed in space, but its previous sediment fill is progressively moved  
65 away from it, producing a characteristic asymmetric, shingled stratal unit (Fig. 1a-  
66 b).

67 A second type of RSB has been identified above salt-detached systems in which  
68 the base of the moving unit is a salt layer (Fig. 1c-d) (e.g. Kwanza Basin, Angola,  
69 Peel et al. 1998; Marton et al. 1998; Jackson et al. 2001). Building on these  
70 studies, Jackson and Hudec (2005) reviewed the processes and kinematics of  
71 RSBs on the Angolan margin using highly schematized sections and 2D seismic  
72 data. These authors described salt-detached RSBs as being formed by translation  
73 of sediments above a salt layer with a basinward-dipping ramp at its base (Fig. 1c-  
74 d). Movement over the base-salt ramp generates downwarp of the supra-salt  
75 carapace, creating accommodation. Moreover, translation over two or more base-



76 salt ramps can generate vertically stacked RSB systems (Jackson and Hudec,  
77 2005).

78 Both the extensional and salt-detached RSBs are characterized by an asymmetric  
79 synclinal depocentre defined by a basinward-dipping axial-trace (Fig. 1) (Jackson  
80 and Hudec, 2005). Thus, sediment layers within RSBs typically dip in the opposite  
81 direction to tectonic transport, defining “pseudo-clinoforms” (Fig. 1). In settings  
82 where the background sedimentation rate ( $\square$ ) is low, the top and bottom bounding  
83 surfaces of the RSB growth package take the form of diachronous unconformities.  
84 The basal boundary is an onlap surface whereas the top boundary is defined by  
85 offlap/toplap geometries. In settings where the background sedimentation rate ( $\square$ )  
86 is relatively high, these surfaces are expressed as diachronous boundaries across  
87 which the sediment thickness abruptly changes from expanded within the RSB, to  
88 normal thickness outside of it (Fig. 1)

89 The dip of the depositional axial-trace defines relative ratios of aggradation ( $\square$ ) and  
90 translation ( $\square$ ) rates (Jackson and Hudec, 2005). Gently-dipping axial traces  
91 indicate low  $\square/\square$  whereas steeply-dipping axial traces indicate high  $\square/\square$ . This ratio  
92 tends to increase through time as translation rates usually decrease due to salt  
93 thinning and thickening of the overburden (Jackson and Hudec, 2005). Although  
94 geometrically similar, extensional and salt-detached RSBs have important  
95 differences in terms of stratal architecture, processes and depositional settings that  
96 will be addressed in detail in this study.

97 The geometry and stratigraphy of RSBs can provide important information on the  
98 evolution of sedimentary basins. They present an excellent and continuous record  
99 of the translation history revealing total duration, displacement distance, speed,  
100 and direction (Hudec and Jackson, 2005). With stratigraphic age control of intra-  
101 RSB intervals, it is possible to identify whether translation rate was uniform or time-  
102 variant, allowing accurate estimates of overburden translation and deformation  
103 rates on salt-detached gravity-driven systems (Jackson and Hudec, 2005). This  
104 can be extrapolated to more structurally complex domains, such as the updip  
105 extensional and downdip contractional provinces, where strain restoration and  
106 kinematic analysis can be problematic (Jackson et al. 2014).

107 Furthermore, in regions where available data do not allow clear imaging of the  
108 base-salt surface or pre-salt stratigraphy, the identification of RSBs may indicate  
109 the presence, geometry and location of pre-salt highs, as RSBs updip edges occur  
110 immediately above them (Fig. 2). This may, in turn, assist the identification of  
111 hydrocarbon targets in pre-salt highs sealed by the salt layer, which are prolific  
112 plays in the deep-waters of South Atlantic basins (Gomes et al. 2012; Flinch, 2014;  
113 Mohriak, 2015). RSBs also control slope and abyssal plain deposition and, thus,  
114 can influence the distribution of hydrocarbon reservoirs in supra-salt intervals. Salt-  
115 detached gravity-driven translation causes a seaward-shift of supra-salt strata,  
116 which can result in juxtaposition of supra-salt sandier intervals deposited on the  
117 shelf and upper-slope, above mature pre-salt source rocks on the lower-slope and  
118 deep-basin (Fig. 2). If a salt weld is formed below the RSB, these supra-salt  
119 reservoirs can be charged by hydrocarbon migration from the pre salt section

120 (Rowan 2004; Jackson et al. 2014). Wherever RSBs are present, one cannot fully  
121 understand supra-salt stratigraphic architecture without understanding the  
122 kinematics of RSBs.

123 Despite the notable value for both academia and hydrocarbon exploration, there  
124 has been little further research on the subject since Jackson and Hudec (2005).  
125 There has been no investigation of RSBs 3D kinematics and stratigraphic  
126 architecture, or physical and numerical modelling. Very few studies documented  
127 RSBs outside their type-area in the Kwanza Basin: Rowan (2014) in the Red Sea  
128 and Dooley et al. (2017) in the Campos Basin, Brazil. Nevertheless, RSBs have  
129 been shown in previous works without being explicitly recognized (Alves et al.  
130 2017; Jackson and Hudec, 2017).

131 Here we present the first ever documentation of RSBs in the Santos Basin, Brazil,  
132 providing for the first time a detailed analysis of their 3D stratigraphic architecture  
133 and kinematics. We present seismic sections and thickness maps of the RSBs  
134 mapped in the Santos Basin and, then, compare their geometries with models that  
135 simulate cover translation above a salt detachment with variable topography and  
136 thickness. These models provide a more comprehensive and realistic evolution of  
137 RSBs, as they treat the detachment as a volume of deforming viscous material  
138 (Fig. 1d-f), rather than a discrete undeformable surface (Jackson and Hudec,  
139 2005). This allows us to evaluate the role of diapirism and salt flux variations on  
140 RSB evolution. Ultimately, this work aims to improve our current understanding of  
141 RSBs and to work as a guide for the identification and analysis of these systems in  
142 other settings and basins.

## 143 **2. Tectono-Stratigraphic Framework of the São Paulo Plateau**

144 The São Paulo Plateau (SPP), Santos Basin (Fig. 3), is an area of thick Aptian salt  
145 characterized by prominent intra-salt layering (Davison et al. 2012; Fiduk and  
146 Rowan, 2012; Jackson et al. 2014; 2015) and a complex, polygonal pattern of salt  
147 diapirs (Guerra and Underhill, 2012; Jackson et al. 2015). The area is a prolific  
148 hydrocarbon province with discoveries on both pre- and post-salt intervals,  
149 including some of the largest oil discoveries in the last decades (e.g. Tupi and  
150 Iracema fields) with reserves over 5 bbl in pre-salt structural highs (Mohriak et al.  
151 2012).

152 The basin is characterized by a series of NE-oriented graben and half-graben  
153 formed during late Barremian-early Aptian rifting. These basins are filled by non-  
154 marine clastic strata and overlain by shallow-marine carbonates (Meisling et al.  
155 2001; Modica and Brush, 2004; Karner and Gambôa, 2007; Mohriak et al. 2008,  
156 2009; Contreras et al. 2010). During the late Aptian, fault activity was reduced and  
157 a 1 - 3 km thick post-rift salt succession was deposited (Davison et al. 2012).  
158 During the early Albian, the Santos Basin experienced fully marine conditions due  
159 to thermally-induced subsidence and eustatic rise, which resulted in widespread  
160 deposition of a carbonate-dominated succession, in the study are expressed as a  
161 fine-grained, marl-dominated succession (Modica and Brush, 2004). During the  
162 latest Albian, thermal and isostatic subsidence tilted the basin south-eastward,  
163 inducing gravity gliding and the development of an array of thin-skinned,  
164 predominantly seaward-dipping salt-detached normal faults that dismembered the  
165 Albian carbonate platform into extensional rafts updip of the study area (Demercian

166 et al. 1993; Cobbold et al. 1995; Mohriak et al. 1995; Guerra and Underhill, 2012;  
167 Quirk et al. 2012).

168 During the Cenomanian-Turonian, drowning of the carbonate platform in response  
169 to a rapid eustatic rise and thermal subsidence resulted in extensive deposition of  
170 shales and marls in the study-area (Modica and Brush, 2004). Throughout the Late  
171 Cretaceous to Paleocene, and despite the continued eustatic rise, sedimentation  
172 was dominated by siliciclastic progradation due to landward uplift of the Serra do  
173 Mar mountain range, with extensive turbidite deposition during the late Campanian  
174 (Modica and Brush, 2004). By the end of the Paleocene, sea-level fall resulted in  
175 the development of a major regional unconformity, leading to erosion of shelf and  
176 slope sediments, and causing their deposition further basinward. Inflated salt on  
177 the SPP acted as a topographic barrier to basinward transportation of coarse  
178 clastics from the end of the Paleocene onward (Modica and Brush, 2004), resulting  
179 in widespread mud deposition.

180 The SPP is situated at the present-day toe-of-slope, immediately downdip of the  
181 Albian extensional domain and the Albian Gap (Fig. 3) (Quirk et al. 2012; Jackson  
182 et al. 2015). Some authors suggest regional shortening of the supra-salt cover in  
183 the SPP continued throughout the late Cretaceous (Quirk et al 2012; Fiduk and  
184 Rowan 2012; Guerra and Underhill, 2012; Alves et al. 2017). Others argue that late  
185 Cretaceous deformation was dominated by salt inflation (Ge et al. 1997; Gemmer  
186 et al. 2004; Jackson et al 2015; Dooley et al 2015). However, there has been no  
187 study so far regarding the aspects and amount of salt-related translation in the  
188 area.

### 189 **3. Methods**

#### 190 **3.1. Seismic Interpretation**

191 This study uses a zero-phase processed, time-migrated, 3D seismic reflection  
192 dataset that covers 20,122 km<sup>2</sup> of the SPP, Santos Basin, Brazil. Inline (west-east)  
193 and crossline (north-south) spacing is 18.75 and 25 m, respectively. Vertical  
194 sampling interval is 4 ms two-way time travel (ms TWT) and total record length  
195 analysed is 5500 ms TWT. The survey display follows the Society of Economic  
196 Geologists normal polarity, where a downward increase in acoustic impedance is  
197 represented by a positive reflection event (white on seismic sections) and a  
198 decrease in acoustic impedance by a negative event (black on grey-scale seismic  
199 section) (Brown, 2011).

200 The dominant frequency in the Aptian salt is c. 30 Hz and the average interval  
201 velocity is 3.4 km/s, which yields a vertical resolution around 25-30 m. The  
202 relatively lower velocity of the salt compared to pure halite is due to the intra-salt  
203 lithological heterogeneity and presence of acoustically slower potash intervals  
204 (Jackson et al. 2015). Overburden sediments have a similar frequency of c. 31 Hz  
205 and a lower average interval velocity (c. 2.0 km/s), which, together result in a much  
206 finer vertical resolution (c. 15-20 m) coarsening with increasing depth and  
207 increasing velocity. Horizontal resolution is twice the seismic line spacing (i.e.,  
208 37.5 m in the E–W direction and 50 m in the N–S direction) (Jackson et al 2015).

209 In order to understand the 3D kinematics and tectonostratigraphic evolution of  
210 RSBs, 3D seismic mapping of key internal horizons was conducted using in in-

211 lines, cross-lines, and in strike- and transport-parallel sections to obtain accurate  
212 estimates of the translation history of these systems. TWT structure maps for top-  
213 salt (Fig. 4) and key surfaces within the RSBs were produced to generate  
214 thickness maps of key stratigraphic intervals.

215 The study did not involve the use of primary well data, or independent picking of  
216 horizon tops in wells. Intra-RSB horizons were chosen as the most distinctive  
217 positive reflections with high amplitude and lateral continuity. Identification of key  
218 seismic stratigraphic surfaces, such as the base and top salt, top Albian, and the  
219 intra-Paleocene unconformity, was based on previous publications (Fiduk and  
220 Rowan, 2012; Guerra and Underhill, 2012; Jackson et al. 2015; Alves et al. 2017).

### 221 **3.2. Base-salt Map**

222 It was vital to have a detailed base-salt map in order to match the observed RSBs  
223 to the base-salt topography responsible for their formation. Although, the top and  
224 base-salt surfaces were readily identified and interpreted in TWT; the presence of  
225 a thick, deformed evaporite layer, whose velocity is higher than the overlying  
226 sediments, introduces distortion of the base-salt and pre-salt section such that the  
227 real structure is obscured by velocity pull-ups. Although, in places, syn-rift  
228 structures (i.e. normal faults and wedge-shaped intervals) helped constraining pre-  
229 salt structures (Figs. 6-7), in other areas these structures could not be readily  
230 identified in an unadjusted TWT base-salt map.

231 Publically available depth-maps (e.g. Alves et al. 2017) do not cover the entire  
232 study area nor do we have access to a reliable, high-resolution velocity grid to

233 create maps by conventional depth-conversion. Instead, we developed a reliable  
234 and applicable base-salt structure map (Fig. 5) by stretching the thickness of salt  
235 by a factor of 1.61 and shifting everything below salt accordingly. This is equivalent  
236 to a static correction, in which the velocity of salt is reduced to 61% of its natural  
237 value. The appropriate substitution factor was obtained by iteration to find the value  
238 that best removes observed pull-up. Finally, a gentle spatial smoothing factor was  
239 applied to remove the effect of non-vertical ray paths, which created local high-  
240 frequency spikes under the steeply-dipping flanks of salt bodies (Jones and  
241 Davison, 2014). The resulting map is in TWT, not depth, and it represents where  
242 the base-salt reflection would be if the salt were replaced by an equivalent  
243 thickness of sediment.

244 The best indicator that the process was effective is that the resulting map (Figure  
245 5a) shows no discernible imprint of the overlying salt structure, and it compares  
246 favourably to depth-maps such as that presented by Alves et al. (2017). Four major  
247 base-salt highs are identifiable on the map; each bounded updip and downdip by  
248 base salt ramps (Fig. 5). This result compares well with the interpretations shown  
249 by Davison et al. (2012) and Alves et al. (2017), both of whom used depth data.

#### 250 **4. Ramp-Syncline Basins in the Santos Basin, Brazil**

251 Several series of simple and stacked RSBs were identified above thick salt (1.5-2  
252 km) in the Sao Paulo Plateau, Santos Basin, distributed above and basinward of  
253 the main base-salt steps in the area (Figs. 4-5). These basins trend NNE to NE  
254 (Figs. 5) and are composed of 9-20 km wide by 15-35 km long continuous panels



255 of landward-dipping and thickening strata that become younger landward (Figs. 6-  
256 10). Base-salt steps trend NNE to NE, parallel to the RSBs, although the  
257 northernmost high trends NNW, oblique to them (Fig. 5) (H2 of Alves et al 2017). In  
258 this study, we present the 5 least deformed, largest, and thus best imaged  
259 examples of RSBs in order to analyse their 3D kinematics, tectono-stratigraphic  
260 evolution, and interaction with diapirism and base-salt structures.

261 The RSBs are characterized by asymmetric sigmoidal strata dipping and  
262 expanding landwards towards a diachronous basal boundary, being capped by a  
263 diachronous top unconformity (Figs. 6-8). Their depositional axial-trace (red  
264 dashed line) dips mainly basinward, becoming progressively steeper at the  
265 uppermost strata, landward (Fig. 6-7). However, viscous salt drag and  
266 synchronous diapirism can bend and rotate RSB intervals, switching the dip  
267 direction of their axial-trace (Fig. 8).

268 These systems contain stratigraphic successions up to 700 ms (~800 m) thick (Fig.  
269 8); with an average vertical thickness of 400 ms (450-500 m, Fig. 7), which  
270 corresponds to only 20-40% of total post-salt succession. However, this does not  
271 represent the true stratigraphic thickness of the RSB fill as these strata have been  
272 rotated by a combination of translation (>20 km) and diapirism (Figs. 6-10).  
273 Thickness maps of intra-RSB intervals indicate a minimum true stratigraphic  
274 thickness varying from 1,670 ms (~ 1,900 m) in RSB 3 (Fig. 8) to 2,130 ms (~  
275 2,400) in RSB 4 (Fig.10).

276 In the majority (85%) of RSBs identified, the first onlapping strata occur against the  
277 top Albian interval (Figs. 6 and 8-10), characterized by a broadly isopachous  
278 section, 300-400 ms (c. 300-400 m) thick, of continuous and low-amplitude  
279 reflections defined at the top by distinctive high-amplitude positive reflections  
280 (Guerra and Underhill, 2012; Jackson et al. 2015). In the other 15% of RSB panels,  
281 the first onlaps are against younger, late Cretaceous strata (Fig. 7). Our  
282 interpretation suggests that this occurs because these systems can be segmented  
283 by salt walls and diapirs (Fig. 8-10). In places, horizon correlation along-strike and  
284 around the diapirs (Fig. 4) shows that the landward panels are composed of  
285 younger strata onlapping a thicker and younger pre-translation section (Fig. 8),  
286 relative to their basinward equivalent panel. This indicates these panels are  
287 genetically linked, comprising a single RSB formed by post-Albian translation  
288 above the same ramp (Fig. 11a-b), and that they were subsequently separated by  
289 syn- to post-translation diapirism. Another evidence of viscous salt drag and  
290 basinward translation in these systems is the development of intra-salt basinward-  
291 vergent shear zones (Figs. 6 and 8).

292 In the north-central and northeast portions of the SPP, RSBs have a distinctly  
293 different geometry compared to those further south. They are characterized by  
294 stacked onlap surfaces and ramp-syncline strata (Figs. 9 and 10), formed by  
295 simultaneous cover translation above two or more base-salt ramps (Jackson and  
296 Hudec, 2005). Each of the stacked RSBs develops by strata translation, rotation,  
297 and bending above a single base-salt step. The lower or landward RSB forms by  
298 translation above the landward ramp, whereas the upper or basinward RSB forms

299 by translation above the basinward ramp (Figs 9, 10 and 11c). If the distance  
300 between the base-salt ramps is smaller than the amount of translation in the  
301 system, the updip portion of the basinward RSB overlaps the downdip portion of  
302 the landward RSB, generating a set of stacked RSBs (Figs. 9-10). Intuitively, the  
303 distance between steps is inversely proportional to the width of the stacked RSB  
304 section. Deposition occurs simultaneously within both stacked RSBs, so the first  
305 and last deposited strata and equivalent onlap points in each RSB have the same  
306 age and, accordingly, the amount of translation in each RSB is the same (see  
307 models, section 4.3) (Jackson and Hudec, 2005).

308 The stratigraphic architecture of stacked RSBs is similar to the individual systems  
309 described previously (Figs. 6-8), with landward-dipping sigmoidal strata defined by  
310 a basinward-dipping axial trace (Figs. 9 and 10). In both cases, stratal termination  
311 can vary along dip and strike. Thus, we present a summary of RSB stratigraphic  
312 architecture and terminations for both the simple and stacked systems (Fig. 11).

313 Lower boundaries are generally characterized by a well-defined, diachronous onlap  
314 surface that becomes younger landward (Figs. 8-10). Apparent downlaps are  
315 typical of the lowermost RSB fill, which has been progressively rotated during  
316 translation, whereas the original onlap relationships are most easily discerned for  
317 the younger landward packages (Figs. 6-10). We thus interpret the apparent  
318 downlaps as being originally formed as onlaps against paleo-bathymetric highs  
319 and/or diapirs above base-salt ramps. These terminations dominate where strata  
320 are older and consequently have been translated and rotated further. Elsewhere,

321 the basal boundary is also defined by transition from thicker, landward-dipping  
322 section to a drape interval at regional dip (Figs. 8-10 and 11b-c).

323 Upper boundaries also become younger landward and are defined in places by  
324 erosional truncation, most commonly in the downdip part of the system where  
325 strata are usually steeper (orange to blue horizons, fig. 7). Steep stratal dips and  
326 erosional truncation are possibly caused by a combination of: i) uplift due to salt  
327 drag (see model in Fig. 8) and/or salt inflation at the edge of the RSB (not  
328 modelled); and ii) a higher degree of translation and rotation of older RSB strata.  
329 Elsewhere, the upper boundary is defined by toplaps (lilac horizon, fig. 7) or,  
330 usually in the updip portions of the system, by an abrupt transition from thin,  
331 draping section with an overall regional dip to a thicker section that dips more  
332 steeply than regional (light orange horizon, Fig. 7).

333 This landward shift from abrupt to subtle, transitional limits along the upper and  
334 lower boundaries of the RSBs (Fig. 11b) is explained by an increase in the ( $\square/\square$ ).  
335 This is evidenced by the landward steepening of the depositional axial-trace in  
336 areas where the RSBs are less folded (Fig. 6-10). Additionally, as the RSB evolves  
337 and the  $\square/\square$  increases, the overburden becomes progressively thicker such that  
338 loading and salt expulsion can act as a secondary control on RSBs evolution.  
339 Thus, salt expulsion and diapirism occur in tandem with translation and RSB  
340 development (Jackson and Hudec, 2005), as seen in portions of our seismic  
341 examples where RSBs have a more symmetric geometry and salt has drastically  
342 thinned beneath them (SE edge of RSB 3, Fig. 8).

343 Vertical juxtaposition of stacked RSBs can complicate their stratal terminations.  
344 The unconformity bounding the top of the lower RSB forms the basal onlap surface  
345 of the upper RSB along most of the stacked section (Figs. 9-10). However, as in  
346 simple RSBs, the boundaries of each stacked system can be defined by transition  
347 from steeper, thickened section within the RSB, to thin, draping strata away from it  
348 (Figs. 9 and 10b). This can result in the development of a thin drape interval  
349 separating the lower RSB top unconformity from the upper RSB onlap surface  
350 (Figs. 9 and 10), which typically occurs in their uppermost sections (Fig. 11c).

## 351 **5. RSB modelling and kinematics**

352 The observations made from seismic interpretation were compared with forward  
353 models reproducing what was interpreted as the main process operating in these  
354 settings, i.e. cover translation above a thick salt detachment. This comparison  
355 allowed us to evaluate the kinematics and processes controlling the development  
356 of RSBs and to confirm that the observed geometries were explicable in the  
357 framework of the interpreted base-salt topography. In such systems, translation of  
358 the cover is accommodated by layer-parallel shearing of the whole thickness of the  
359 salt, i.e. Couette flow (Weijermars, 1993; Rowan et al. 2004) as opposed to  
360 movement on a fault (McClay, 1990; 1996) or a discrete detachment surface  
361 (Jackson and Hudec, 2005).

362 Modelling was performed using a novel application, SaltDragon®, created in  
363 Microsoft Excel®. This application provides a simple but effective 2D model of the  
364 stratal geometries produced in RSB systems by simulating viscous salt drag and

365 overburden translation above a thick salt detachment with variable thickness and  
366 basal topography. The geometry of the decollement and the rate of sediment  
367 accumulation can be adjusted in order to replicate the general form of the natural  
368 RSBs observed on seismic data, and to investigate the possible controls on RSB  
369 geometry. The application is non-dimensional, i.e. scaling-independent: the  
370 computations relate to grid cells, and are valid regardless of the dimension of the  
371 grid, or of the vertical scaling factor.

372 The overburden is offset horizontally, one grid cell per time increment, over the  
373 viscous decollement, with an initially uniform top and a base of user-defined  
374 irregularity, while the pre-salt interval remains fixed and rigid. The post-salt pre-  
375 translation interval is represented by a tabular package and syn-kinematic  
376 sedimentation is continuous and at a constant rate through time. After each  
377 increment, the overburden is deformed by vertical shear to maintain contact with  
378 the top of the salt. The height of the new sediment depositional surface at each  
379 point in time is user-defined. The calculated accommodation (space between the  
380 new depositional surface and the top surface of the deformed overburden)  
381 determines the thickness of new sediment deposited in each increment. There is  
382 no compaction and erosion in this model and the depositional surface is presumed  
383 to be planar and uniformly dipping, which is likely applicable to the deep-water  
384 settings considered in our natural examples. The process is repeated sequentially,  
385 creating a complete realisation of the evolution of the system.

386 The shear strain associated with the layer-parallel shearing within the salt is  
387 assumed to be uniform throughout each vertical column (Fig. 12). Thus, where salt

388 is thinner, the total flux of dragged salt is lower than where the salt is thicker and  
389 *vice versa* (Fig. 12) (Dooley et al. 2017). As the original salt thickness changes  
390 across base-salt topography, the overall salt flux also changes. As a result, parts of  
391 the section may experience net loss or gain of salt, resulting in salt thickness  
392 variations and subsidence or uplift of the overlying sediments (Fig. 12). This  
393 controls the deposition and stratigraphic architecture of syn-kinematic strata, and  
394 the development of RSBs.

395 Because the models begin with a planar top-salt surface; in its initial stages, the  
396 generation of subsidence and uplift is entirely due to the effect of salt drag and  
397 laterally varying salt flux (Figs. 12a-b). However, as the model evolves, significant  
398 topography is created on the top salt surface and a second factor comes into play.  
399 The cover, then, moves with a downward component where the top-salt dips in the  
400 direction of tectonic transport, and has an upward component where the top of salt  
401 dips in the opposite direction (Figs. 12c). This produces components of local  
402 subsidence and uplift, in addition to those created by local depletion or increase in  
403 salt thickness. An important consequence of this is that regions of local uplift can  
404 develop in the downdip side of RSBs even where the cover is moving over a  
405 basinward-dipping ramp (Fig. 13c-d).

406 As the top-salt topography develops, the amount and extent of uplift should  
407 progressively increase (Figure 13c-d). In nature, a combination of Couette and  
408 Pouiseuille salt-flow would intensify the uplift as salt would be laterally expelled  
409 from beneath the RSB resulting in inflation and diapirism at its edges. If the system  
410 experiences very large lateral displacement, we would expect the salt layer

411 thickness to become near-uniform, as differential Couette drag tends to  
412 progressively even out the initial variation in salt thickness.

413 We present 4 models where we test the effects of different base-salt topography  
414 and variable salt thickness on overburden translation. Model 1 simulates  
415 translation above a basinward-dipping ramp and model 2 reproduces translation  
416 above a pair of basinward-dipping ramps. In Model 3, we evaluate translation over  
417 a landward-dipping ramp and in Model 4, translation over a base-salt high (horst  
418 block), with a landward- and basinward-dipping ramp.

419 Whilst the models appear to reproduce actual geometries observed in salt basins,  
420 they do not reproduce the entire kinematics and other salt-related processes that  
421 operate in RSB systems, such as diapirism and Poiseuille-flow driven by  
422 differential loading. Also, it makes the assumption that: 1) the overburden neither  
423 stretches nor shortens laterally as it moves or, 2) the sediment layer has very little  
424 resistance to vertical shear, so there is no salt return Poiseuille-flow component, as  
425 would be the case with a more rigid roof. Nevertheless, separating the contribution  
426 of one factor alone (entrainment of the viscous decollement layer by drag,  
427 modelled as Couette flow) allows us to explore the influence of this important  
428 component of salt tectonics. Furthermore, the fact that this approach produces  
429 results that are remarkably similar to RSBs observed in both Santos and Kwanza  
430 Basins, suggests it is a valid first-order approximation of their dynamics.

### 431 **5.1. Model 1 (Basinward-dipping ramp)**



432 In Model 1, salt and overburden translate over a basinward-dipping ramp. As salt is  
433 thinner updip of the step (Fig. 13), less salt is dragged into the step than out of it  
434 (Dooley et al. 2017). This salt deficit results in local salt thinning and cover  
435 subsidence (Fig. 12a and 13a-b), and the generation of an asymmetric depocentre  
436 above the ramp. As translation continues, previously deposited strata are moved  
437 out of the ramp while new sediments are deposited immediately above it. This  
438 results in the development of a RSB, characterized by an asymmetric growth  
439 interval that dip and expand landwards towards a diachronous basal boundary,  
440 being truncated above by a diachronous unconformity (Fig. 13c-d), similar to  
441 natural examples from the SPP (Fig. 6).

442 The axial-trace and bounding surfaces are sub-parallel to each other (Fig. 13d).  
443 Initially, they dip gently in the direction of tectonic transport, i.e. basinward (Fig.  
444 13b) but as translation progresses, salt drag and uplift rotate these surfaces,  
445 flipping their dip direction, i.e. landward, at the downdip edge of the system (Fig.  
446 13c and d). Because in the model translation and sedimentation rates are constant,  
447 this change in geometry happens entirely in response to shear drag and the  
448 consequent upward translation and rotation of syn-kinematic strata. In reality,  
449 folding and rotation of RSBs internal intervals and surfaces can be even more  
450 pronounced due to a combination of: i) variations in  $\mu/\rho$ , ii) salt expulsion and  
451 diapirism, and ii) extension and contraction.

452 Basal surfaces of salt-detached RSBs are usually diachronous and shingled (i.e.  
453 not a discrete surface as in extensional RSBs) as sediments may also be  
454 deposited upslope of the RSB in the form of a thin drape fringing the main

455 depocentre (Fig. 13c and d). In our seismic examples, thin drape horizons usually  
456 occur at the updip portions of the systems, being usually 1-2 seismic reflections  
457 thick (Fig. 9), equivalent to only a few tens of meters.

458 Model 1 is also run with a higher  $\alpha/\beta$  to illustrate how varying the relative rates of  
459 aggradation and translation produces different RSB stratal architectures (Fig. 14).  
460 Translation rate ( $\beta$ ) is kept constant while aggradation rate ( $\alpha$ ) is increased 3-fold  
461 (Fig. 14b). When the  $\alpha/\beta$  is low, the RSB geometry is more asymmetric and its  
462 boundaries are defined by abrupt strata terminations (Fig. 14a). Conversely, when  
463 the  $\alpha/\beta$  is high, there is less asymmetry, the synclinal axial-trace is steeper, and  
464 strata terminations are characterized by a transition from a thicker, steeper section  
465 within the RSB to thinner intervals at regional dip outside of it (Fig. 15b). If  $\alpha$  is  
466 higher than  $\beta$ , local uplift in the downdip side of the RSB is not enough to generate  
467 sea-floor exposure and erosion (Fig. 12c and 14b), which in a deep-water setting as  
468 in the SPP, could be driven by bottom currents. Although not shown here,  
469 variations of sedimentation rate during the development of RSBs can also produce  
470 intra-RSB unconformities and offlap terminations.

## 471 **5.2. Model 2 (Two Basinward-dipping ramps)**

472 Model 2 simulates cover translation above a thick salt layer with two closely-  
473 spaced base-salt basinward-dipping ramps (Fig. 15). Basin geometry and evolution  
474 above each base-salt ramp is similar to Model 1, such that a landward RSB forms  
475 above the landward ramp while a basinward RSB develops above the basinward  
476 ramp (Fig. 15b-c). As translation continues, these basins are vertically juxtaposed

477 forming stacked RSBs (Fig. 15c-d) as in our seismic examples (Figs. 9-10).  
478 Deposition occurs simultaneously within both RSBs (Fig. 15b-d), which means the  
479 first and last deposited strata and respective onlap points in each of the stacked  
480 RSBs have the same age and, accordingly, record the same amount of translation  
481 (Fig. 15) (Jackson and Hudec, 2005).

482 The most basinward interval of each RSB corresponds to older strata that have  
483 translated further, thus, being more rotated and uplifted by shear drag than  
484 younger intervals (Fig. 15). If the aggradation rate is lower than salt movement  
485 rate, salt drag results in exposure of the basinward side of each RSB (Fig. 15d),  
486 leading to localized erosion, as seen in natural examples (landward and basinward  
487 RSBs in fig. 10 and landward RSB in Fig. 9). The width of the exposed area is  
488 smaller in the landward RSB, presumably because it is progressively and partially  
489 buried by the basinward RSB strata, onlapping onto the landward RSB top  
490 unconformity (Fig. 15d).

491 Our model shows that the lower, landward RSB top unconformity acts as the basal  
492 onlap surface of the upper, basinward RSB (dashed black line in fig 15d), as seen  
493 in seismic examples (Figs. 9 and 10). When the sedimentation rate is lower than  
494 the translation rate, the stacked RSBs top unconformities merge landward, and  
495 their basal onlap surface merge basinward (Fig. 15). Although there is a level of  
496 uncertainty due to the presence of folds and diapirs in the study area, this pattern  
497 is seen in portions of RSB 5 (Fig. 10 a-b), where the RSB interval is thinner. When  
498 sedimentation rate is relatively higher, a thin drape interval can separate these  
499 boundaries (Fig. 9).

500 As seen in the model each RSB finishes landward above the top of its respective  
501 ramp (Fig. 15d). This is seen throughout most of our seismic examples (LW ramp  
502 and middle ramp RSBs in Fig. 10) although in some areas, diapirism and  
503 overburden deformation can laterally offset their landward edge from the top of  
504 their respective ramps by up to 1-2 km (Fig. 9). These complexities, however, lead  
505 to only a minor amount of uncertainty when compared to the total translation and  
506 extent of these systems (see section 4.5) and, thus, are not enough to invalidate  
507 translation estimates.

### 508 **5.3. Model 3 (Landward-dipping Ramp)**

509 Model 3 simulates cover translation above a thick salt detachment with a landward-  
510 dipping basal step and generates similar syn-kinematic stratal geometries to Model  
511 1. However, this time, the RSB forms immediately basinward of the step, above a  
512 base-salt flat (Fig. 15), instead of above the step as in Model 1 (Fig. 16). As salt  
513 moves from an area of thick to thin salt across the ramp, salt streamlines converge  
514 so that more salt is dragged into the ramp than out it (Figs, 12b and 16a-b) (Dooley  
515 et al. 2017). This salt surplus results in salt thickening and cover uplift above the  
516 step, and generation of accommodation around the salt anticline formed over the  
517 ramp.

518 As translation continues, more salt is fed into the anticline causing it to widen  
519 basinward without leaving its original position. Thus, whilst its landward flank  
520 remains static, the basinward flank translates and acts similarly to a basinward-  
521 dipping ramp forming an asymmetric depocentre above it. Syn-kinematic strata

522 onlap and thicken towards this flank while being progressively rotated and  
523 translated basinward (Fig. 16b-c).

524 The evolution and geometry of the asymmetric growth interval are notably similar  
525 to RSBs formed above basinward-dipping ramps (compare Figs. 13 and 16) and to  
526 natural examples of RSBs formed above landward-dipping steps (Figs. 7 and 8).  
527 These RSBs are composed of shingled sigmoidal strata that dip and expand  
528 landward, being located basinward of a landward-dipping base-salt step and above  
529 a base-salt flat (Figs. 7 and 8). They are bound on their landward edge by a wide  
530 diapir (Fig. 7) or a salt anticline (Fig. 8) that is situated directly above the top of the  
531 ramp, as in the model (Fig. 16).

532 In the model, the salt anticline remains static but, in reality, it can abandon the  
533 ramp after reaching enough topography and gravitational instability, being  
534 translated downdip while a younger salt structure forms above the ramp. After  
535 leaving the ramp, the structure will probably experience extensional reactivation as  
536 the system accelerates, as shown in physical models (Dooley et al. 2017) and  
537 seismic examples (mid-RSB diapirs in Fig. 9). As the anticline grows and its roof is  
538 uplift, outer-arc extension and erosion (not modelled) can thin the roof and allow  
539 diapiric piercement as seen in RSB 2 (Fig. 7).

540 The apparent offset of synkinematic strata across the diachronous onlap surface  
541 above the anticline could be erroneously interpreted as a basinward-dipping listric  
542 fault (Fig. 15c-d). However, it is clear from natural examples and models that this  
543 geometry is entirely formed in response to differential uplift and sedimentation

544 during cover translation. As salt thickens above the ramp, sediments are deposited  
545 around the anticline while the area above it remains sediment starved (Fig. 15). As  
546 translation progresses and the anticline widens, the landward section is translated  
547 over the structure, while the basinward section translates further basinward (Fig.  
548 15c-d). Ultimately, this will result in an apparent offset that is equal to the width of  
549 the diapir (Fig. 15c-d), but which is clearly not associated with faulting.

#### 550 **5.4. Model 4 (Base-Salt High)**

551 Model 5 illustrates the development of stacked RSBs formed by translation over a  
552 base-salt high akin to a horst block defined by a landward-dipping ramp updip and  
553 a basinward-dipping ramp downdip (Fig. 17), as in RSB 5 (Fig. 10). Each step  
554 works as in previous models. Translation across the landward step results in salt  
555 thickening above the step and development of a RSB basinward of it, whereas  
556 translation over the basinward step results in salt thinning and subsidence with  
557 generation of another RSB above it. As translation progresses these minibasins  
558 overlap and a stacked RSB system forms.

559 Whereas the basinward RSB is very similar to previous models of basinward-  
560 dipping ramps (Figs. 13 and 17), the geometry of the landward RSB is different  
561 when compared to the previous model of a RSB formed above a landward-dipping  
562 ramp. Because the landward RSB moves over the second, basinward-dipping step,  
563 it subsides and rotates further, thus, having a steeper, basinward dip (Fig. 17). This  
564 is seen in RSB 5 where the lower, landward RSB is steeper above the basinward-  
565 dipping ramp, being limited by a wide (>5 km) salt wall (Fig. 10).

## 566 **5.5. Translation history and depocentre migration**

567 To analyse the tri-dimensional kinematics and evolution of the RSBs mapped, we  
568 present true-stratigraphic thickness maps from one RSB (RSB 5, figs. 10 and 18).  
569 These maps have similar trends and shapes for each mapped interval; and  
570 consistent amount (1.8-3 km) and direction of offset ( $120 \pm 15^\circ$ ) through time Fig.  
571 18), which indicate they are formed in response to a single and relatively steady  
572 process, i.e. translation. The consistent offset towards the SE to ESE is roughly  
573 perpendicular to the main base-salt steps and parallel to the regional gravity-driven  
574 tectonic transport direction (Quirk et al 2012; Jackson et al 2014). The depo-thicks  
575 of all five RSBs presented in this study are located basinward or above base-salt  
576 ramps (Fig. 18).

577 By summing the offsets between the thickest points on each map of fig. 18, a total  
578 translation of 26.9 km was obtained. However, this measure does not represent the  
579 total translation of this basin as we do not present thickness maps for the first and  
580 last onlapping intervals. Due to limited seismic resolution and uncertainties related  
581 to salt-related faulting and folding (Fig. 10), it was not possible to generate  
582 accurate thickness maps of these intervals in none of the RSBs mapped.  
583 Nevertheless, it was possible to obtain confident estimates of translation within  
584 these systems by comparing thickness maps with multiple dip-oriented cross-  
585 sections (Figs. 7-10), where we measured the distance of the first onlap point to  
586 the top of the ramp, a methodology also used by Jackson and Hudec (2005).

587 RSB 5 demonstrates the larger amount of overall translation in the SPP, estimated  
588 as 32 km (Fig. 10 and 18). In many other examples, we were only able to  
589 determine a minimum translation because they are located at the eastern edge of  
590 the data, such as in RSB 1 (9.5 km of translation), RSB 2 (18 km) and RSB 4 (16  
591 km); or are eroded or heavily deformed by diapirism. Nonetheless, less-deformed  
592 and less-eroded examples situated far from the edges of the data allowed more  
593 precise estimates of cover translation in the area, which vary from 28 km in the  
594 south (RSB 3, fig. 8) to 32 km to the north (RSB 5, fig. 11). Stacked RSBs were  
595 important to guarantee a higher degree of certainty in areas of complex salt  
596 deformation or intense erosion, because they record the same amount of  
597 translation (Jackson and Hudec, 2005) and, thus, can be used as a cross-check.  
598 As seen in RSB 5, both the landward and basinward RSBs present 32 km of  
599 translation (Fig. 11).

600 Using age constraints provided Modica and Brush, 2004; Guerra and Underhill,  
601 2012; Jackson et al. 2015, it was possible to confirm the time of onset of translation  
602 as being Top-Albian; and to estimate the end of translation to vary from top-  
603 Cretaceous (Fig. 8) to mid-Paleocene (Fig. 7, 9 and 10). Although there is a small  
604 degree of uncertainty regarding these age estimates, we can obtain an  
605 approximate average translation rate of 0.7 – 0.9 mm/yr.

## 606 **6. Discussion**

### 607 **6.1. Extensional vs. salt-related RSBs**



608 Classical RSBs (Fig. 1a-b), are generated by regional extension, in which the  
609 controlling fault cuts progressively downwards through pre-kinematic strata.  
610 Consequently, this interval appears both above and below the fault. The basal  
611 boundary is, thus, defined by an extensional rollover composed of pre-kinematic  
612 strata and a fault surface that is formed at the onset of translation and maintain its  
613 original geometry through time (Fig. 1a-b). The pattern of vertical movement of the  
614 hangingwall is controlled by the shape of the extensional fault. As a consequence,  
615 the geometry and location of the subsiding minibasin does not change as the  
616 system evolves, and the rate of subsidence is directly proportional to the rate of  
617 lateral translation. Therefore, in an extensional RSB, translation of the cover can  
618 result in subsidence, but not in uplift (Fig. 1a-b).

619 In contrast, salt-detached RSBs are not directly driven by extension. Instead, they  
620 form by cover translation above salt (Fig. 1c-d), which, in turn, occurs in response  
621 to gravity-driven extension updip and is linked to contraction or salt advance  
622 downdip (Jackson and Hudec, 2005; Jackson et al 2015). The basal slip surface is  
623 stratabound, i.e. parallel to the pre-kinematic stratigraphy (Jackson and Hudec,  
624 2005), so pre-kinematic strata always occur below their basal surface (Fig. 1c-d).  
625 The base-salt relief is usually related to inherited topography due to previous  
626 basement faulting (Davison et al. 2012); so translation and RSB development are  
627 decoupled from pre-salt deformation.

628 Movement takes place by shearing of a slip volume (viscous salt) rather than a  
629 discrete slip surface (extensional fault in classical RSBs) (Fig. 1c-d). Thus, salt  
630 drag, expulsion and diapirism generate vertical movements, additional

631 accommodation and complexities not observed in extensional systems. The shape  
632 and size of the subsiding minibasin changes as the system evolves, because the  
633 geometry and thickness of the salt detachment vary as the cover moves.  
634 Additionally, as the RSB evolves with increasing displacement, vertical movement  
635 of the surface may change from laterally variable subsidence, to subsidence plus  
636 local uplift (Fig. 1c-d).

## 637 **6.2. Kwanza vs. Santos Basin RSBs: thin vs. thick salt RSBs**

638 In the Kwanza Basin, RSBs formed by 23-26 km of salt-detached translation over a  
639 major base-salt step (Atlantic Hinge Zone), in response to extension further updip  
640 (Fig. 19) (Peel et al. 1998, Hudec and Jackson, 2004, Jackson and Hudec, 2005;  
641 Peel 2014). These RSBs consist of a synclinal growth interval that dips and  
642 expands landward (E-ENE) towards a diachronous basal boundary that becomes  
643 younger and steeper landward (Fig. 19). They are defined by a basinward-dipping  
644 axial trace that also becomes steeper landward and their updip edge occurs  
645 immediately above a base-salt basinward-dipping ramp (Jackson and Hudec,  
646 2005; Peel 2014). This geometry, stratigraphic architecture and relationship with  
647 base-salt topography are notably similar to the examples shown in the SPP,  
648 Santos Basin (Figs. 6-10).

649 However, RSBs in the SPP (Figs. 6-10) have a more complex stratigraphic  
650 architecture, with pronounced folding and rotation of syn-kinematic strata, when  
651 compared to similar systems in the Kwanza Basin (Fig. 19). This contrast is  
652 explained by the stronger effects of synchronous to late diapirism deforming and

653 segmenting RSBs in the SPP, which, in turn, are related to the differences in salt  
654 thickness between the two basins (compare salt thickness between Figs. 3b and  
655 19). In the Kwanza Basin, RSBs are present above a relatively thin (>1 km, Peel  
656 2014), and, now exhausted/welded salt layer; and most of the diapirs were already  
657 developed prior to the onset of translation (Jackson and Hudec, 2005). Salt was  
658 already relatively thin at the onset of translation (Fig. 19a) and a combination of  
659 layer-parallel shearing and salt expulsion beneath the RSB lead to its dramatic  
660 thinning and welding over the ramp, and consequent inflation further basinward  
661 (Fig. 19b-c). This inhibited vertical salt movements and diapirism during translation  
662 and generation of RSBs.

663 Across the Atlantic, in the SPP, the RSBs are now present above thick (>2 km),  
664 layered salt and pre-translation salt structures are rare, with most diapirs forming  
665 during translation and development of RSBs (Figs. 6-10), i.e. post-Albian (Fiduk  
666 and Rowan, 2012; Jackson et al. 2015). Despite the relatively large thickness of  
667 salt detachment, intra-salt layering favoured intra-salt layer-parallel shearing (i.e.  
668 Couette flow), which was accommodated in intra-salt detachment horizons and by  
669 seaward-vergent shear zones (Figs. 6-8). Sedimentation within RSBs above thick  
670 salt imposed an additional loading into the source-layer immediately beneath the  
671 RSB, expelling salt to its surroundings and promoting diapirism (Figs. 8-10), which  
672 become increasingly important through time as the overburden thickens (Jackson  
673 and Hudec, 2005). Thus, synchronous diapirism acted as a stronger second-order  
674 control in RSB evolution in the SPP than in the Kwanza Basin, which resulted in

675 higher degree of folding, rotation and localized erosion (Figs. 8-10), which can  
676 obliterate RSBs original geometries.

677 Another important contrast between these two basins regards the timing and rate  
678 of translation. In the Kwanza Basin, the RSBs are capped by the seafloor at their  
679 landward edges, which demonstrates ongoing activity (Fig. 19) (Jackson and  
680 Hudec, 2005). However, when translation started remains unclear (Jackson and  
681 Hudec, 2005). These authors estimate that translation over the Atlantic Hinge Zone  
682 and development of RSBs initiated in the mid Miocene. This would correspond to a  
683 total translation time of 12-13 Myr at a rate of 2 mm/year, which is surprisingly 2-4  
684 times higher than typical deformation rates of salt-detached gravity-driven systems  
685 (Rowan et al. 2004).

686 In the SPP, however, translation and RSB generation started at the end of the  
687 Albian and stopped during the early- to mid Paleocene (Figs. 6-10). As translation  
688 varied from 28 km to 32 km, movement occurred at an approximate rate of 0.7 –  
689 0.9 mm/year. These are relatively fast, but comparable to deformation rates  
690 measured in Gulf of Mexico (0.1 – 0.5 mm/yr) and Kwanza Basin (0.4-0.5 mm/yr)  
691 (Rowan et al. 2000; 2004). Although, the amount and pattern of translation  
692 between the two basins is remarkably similar, the difference in timing and rate is  
693 thus considerable. We still do not fully understand these contrasts but we believe  
694 that, due to the nature of the 2D data and the limited well-control from the earlier  
695 work of Jackson and Hudec (2005), their estimate of when translation began in the  
696 Kwanza Basin may be inaccurate. A similar and more recent study from these  
697 authors (Dooley et al. 2017) shows one RSB from the Campos Basin, Brazil, where

698 translation started at the end of the Albian as in the SPP, supporting our  
699 interpretation.

700 Why translation is still ongoing in the Kwanza Basin and stopped in the Santos  
701 Basin is out of the scope of this study, as this would require a more regional  
702 analysis involving transects comprising the whole extent of the salt basins in both  
703 margins. However, a few factors can explain why translation ceased in the SPP: 1)  
704 the mobile salt interval, i.e. halite, represented by the transparent seismic facies  
705 within the salt, thinned dramatically in between diapirs (Figs. 6-9), reducing mobility  
706 of the system; 2) dip reversal of the detachment due to the enormous sedimentary  
707 loading associated with the Albian Gap landward of the SPP (Fig.3) (Davison et al.  
708 2012); and 3) the system reached the contractional domain as it is now located at  
709 the toe-of-slope (Fig.3b).

### 710 **6.3. Occurrence of RSBs in other salt basins**

711 There are currently very few publications describing salt-related RSBs. Apart from  
712 Rowan (2014) and Dooley et al. (2017), who briefly describe RSBs in the Red Sea  
713 and Campos Basin, respectively; all previous studies refer exclusively to RSBs in  
714 the Kwanza Basin, (Marton et al. 1998, Peel et al. 1998; Jackson and Hudec,  
715 2005). The question that remains is; therefore, how widespread are salt-related  
716 RSBs?

717 We believe that because of their unique and complex stratigraphic architecture, the  
718 very limited literature about the subject, the lack of a detailed 3D analysis and  
719 modelling of these features, and because they are commonly affected by other salt

720 tectonic processes, RSBs have been previously overlooked. As an example of their  
721 occurrence in other salt basins, we present a 2D seismic profile through a RSB  
722 formed above allochthonous salt in the Essaouira-Agadir Basin, offshore Morocco  
723 (Fig. 20).

724 In the western portion of the section, there is a clear example of a RSB formed  
725 above thick (~1 km) allochthonous salt with a basinward-dipping ramp at its base.  
726 The RSB is characterized by asymmetric and gently folded strata thickening and  
727 dipping mainly landward towards a diachronous basinward-dipping onlap surface.  
728 The system is defined by a steep basinward-dipping axial trace and onlap stratal  
729 terminations that grade upward into transitional boundaries (Fig. 12), a geometry  
730 characteristic of systems with relative high  $\Delta/\Delta$ . Total translation recorded is 9.4  
731 km during Paleocene to Pliocene times, equivalent to rates of 0.15-0.2 mm/year,  
732 comparable with previous estimates of salt translation rates (Rowan et al. 2004).

733 The RSB is bounded updip by extensional domain with normal faults and an  
734 extensional rollover and downdip by an inflated salt tongue that was formed early  
735 by open-toe advance with late folding and uplift during the final stages of evolution  
736 of the RSB (Fig. 20). There is also another potential candidate for an RSB  
737 occurring further updip but the seismic data quality in this part of the section  
738 renders the interpretation of the updip RSB and its causal ramp somewhat  
739 speculative.

## 740 **7. Conclusion**

741 We mapped and presented detailed descriptions and thickness maps of salt-  
742 detached RSBs formed above thick (> 2 km) salt in the São Paulo Plateau, Santos  
743 Basin, Brazil. We compared our seismic interpretation to forward models simulating  
744 cover translation and viscous salt drag above variable base-salt topography to  
745 analyse the kinematics and sequential evolution of RSBs and, explain their  
746 geometries and relationship with base-salt topography.

747 In the SPP, RSBs show consistent magnitudes of total translation, varying from 28  
748 to 32 km; and movement direction, which varies from ESE to SE. We have  
749 demonstrated that these systems have similar geometries, stratigraphic  
750 architecture and relationship to base-salt steps when compared to previously  
751 published examples from the Kwanza Basin (Jackson and Hudec, 2005, Peel  
752 2014). However, in the SPP, ramp-syncline basins are generally more complex  
753 because they occur above thick salt and, consequently, are more affected by  
754 synchronous diapirism and salt-related deformation. We have also demonstrated  
755 that cover translation above landward-dipping ramps can generate notably similar  
756 stratal geometries to classical examples of RSBs formed above basinward-dipping  
757 ramps and that these systems exist in the south-central segment of the SPP.

758 As seen from seismic examples and models, there is a direct relationship between  
759 RSB evolution and base-salt topography, as RSBs finish updip above the top of  
760 base-salt ramps, or above diapirs formed over the ramp. Thus, mapping of RSBs  
761 can aid in the identification of pre-salt structures, being extremely useful in areas of  
762 limited data or limited sub-salt data quality when exploring for sub/pre-salt  
763 exploration targets. Ultimately, this study improves our current knowledge of RSBs,

764 working as a guide for seismic interpretation and recognition of these systems in  
765 other salt basins around the world in the future.

## 766 **8. Acknowledgements**

767 We wish to thank Jonathan Redfern, Mike Hudec, Gillian Apps, Emma Finch and  
768 Sian Evans for sharing their insights and criticisms. We thank CGG for providing  
769 access to the 3D seismic dataset used in this study as well as ONHYM for allowing  
770 us to use one seismic section offshore Morocco. The main author would also like to  
771 thank the Science without Borders program and CNPq, Brazil for sponsoring his  
772 PhD research. Schlumberger is also acknowledged for provision of Petrel software  
773 to the University of Manchester.

## 774 **9. References**

775 Alves, T. M., Fetter, M., Lima, C., Cartwright, J. A., Cosgrove, J., Gangá, A, &  
776 Strugale, M. (2017). An incomplete correlation between pre-salt topography, top  
777 reservoir erosion, and salt deformation in deep-water Santos Basin (SE  
778 Brazil). *Marine and Petroleum Geology*, 79, 300-320.

779 Barton, N., 2007. Rock quality, seismic velocity, attenuation and anisotropy. CRC  
780 press.

781 Benedicto, A., Séguret, M., & Labaume, P. (1999). Interaction between faulting,  
782 drainage and sedimentation in extensional hanging-wall syncline basins: Example  
783 of the Oligocene Matelles basin (Gulf of Lion rifted margin, SE France). *Geological*  
784 *Society, London, Special Publications*, 156(1), 81-108.



785 Carminatti, M., Wolff, B. & Gamboa, L. (2008). New exploratory frontiers in Brazil.  
786 In 19th World Petroleum Congress. World Petroleum Congress.

787 Contreras, J., Zühlke, R., Bowman, S., & Bechstädt, T. (2010). Seismic  
788 stratigraphy and subsidence analysis of the southern Brazilian margin (Campos,  
789 Santos and Pelotas basins). *Marine and Petroleum Geology*, 27(9), 1952-1980.

790 Cobbold, P. R., Szatmari, P., Demercian, L. S., Coelho, D., & Rossello, E. A.  
791 (1995). Seismic and experimental evidence for thin-skinned horizontal shortening  
792 by convergent radial gliding on evaporites, deep-water Santos Basin, Brazil. *In:*  
793 Jackson, M. P. A., Roberts, D. G., Snelson, S. (eds) *Salt tectonics: a global*  
794 *perspective*. AAPG Memoir 65, 305-321.

795 Demercian, S., Szatmari, P., & Cobbold, P. R. (1993). Style and pattern of salt  
796 diapirs due to thin-skinned gravitational gliding, Campos and Santos basins,  
797 offshore Brazil. *Tectonophysics*, 228(3-4), 393-433.

798 Duval, B., Cramez, C., & Jackson, M. P. A. (1992). Raft tectonics in the Kwanza  
799 basin, Angola. *Marine and Petroleum Geology*, 9(4), 389-404.

800 Ellis, P. G., & McClay, K. R. (1988). Listric extensional fault systems-results of  
801 analogue model experiments. *Basin Research*, 1(1), 55-70.

802 Davison, I., Anderson, L., & Nuttall, P. (2012). Salt deposition, loading and gravity  
803 drainage in the Campos and Santos salt basins. *Geological Society of London*  
804 *Special Publications*, 363(1), 159-174.

805 Dooley, T. P., Jackson, M. P., Jackson, C. A. L., Hudec, M. R., & Rodriguez, C. R.  
806 (2015). Enigmatic structures within salt walls of the Santos Basin—Part 2:  
807 Mechanical explanation from physical modelling. *Journal of Structural Geology*, 75,  
808 163-187.

809 Dooley, T. P., Hudec, M. R., Carruthers, D., Jackson, M. P., & Luo, G. (2016). The  
810 effects of base-salt relief on salt flow and suprasalt deformation patterns—Part 1:  
811 Flow across simple steps in the base of salt. *Interpretation*, 5(1), SD1-SD23.

812 Fiduk, J. C., & Rowan, M. G. (2012). Analysis of folding and deformation within  
813 layered evaporites in Blocks BM-S-8 &-9, Santos Basin, Brazil. *Geological Society,*  
814 *London, Special Publications*, 363(1), 471-487.

815 Ge, H., Jackson, M. P., & Vendeville, B. C. (1997). Kinematics and dynamics of  
816 salt tectonics driven by progradation. *AAPG bulletin*, 81(3), 398-423.

817 Gemmer, L., Ings, S.J., Medvedev, S. and Beaumont, C. (2004). Salt tectonics  
818 driven by differential sediment loading: stability analysis and finite-element  
819 experiments. *Basin Research*, 16(2), 199-218.

820 Gibbs, A. D. (1984). Structural evolution of extensional basin margins. *Journal of*  
821 *the Geological Society*, 141(4), 609-620.

822 Guerra, M. C., & Underhill, J. R. (2012). Role of halokinesis in controlling structural  
823 styles and sediment dispersal in the Santos Basin, offshore Brazil. *Geological*  
824 *Society, London, Special Publications*, 363(1), 175-206.

825 Flinch, J., 2014. Context, challenges, and future of deep-water plays: an overview.  
826 Search and Discovery Article, 41417.

827 Gomes, P.O., Kilsdonk, B., Grow, T., Minken, J. & Barragan, R. (2012). Tectonic  
828 evolution of the outer high of Santos basin, southern Sao Paulo Plateau, Brazil,  
829 and implications for hydrocarbon exploration. *In: Gao, D. (eds) Tectonics and*  
830 *Sedimentation: Implications for Petroleum Systems*. AAPG Memoir 100, 125–142.

831 Hudec, M. R. & Jackson, M. P. A. (2004). Regional restoration across the Kwanza  
832 Basin, Angola: Salt tectonics triggered by repeated uplift of a metastable passive  
833 margin. *AAPG bulletin*, 88(7), 971-990.

834 Jackson, M. P. A. & Cramez, C. (1989). Seismic recognition of salt welds in salt  
835 tectonics regimes. *In: Gulf of Mexico salt tectonics, associated processes and*  
836 *exploration potential: Gulf Coast Section SEPM Foundation 10th Annual Research*  
837 *Conference*, 66-71.

838 Jackson, M. P. A., Hudec, M. R., Fraenkl, R., Sikkema, W., Binga, L. & Da Silva, J.  
839 (2001). Minibasins translating down a basement ramp in the deepwater monocline  
840 province of the Kwanza Basin, Angola [abs.]. *In: American Association of*  
841 *Petroleum Geologists Annual Meeting Official Program*, 10, A99.

842 Jackson, M.P. & Hudec, M.R. (2017). Salt Tectonics: Principles and Practice.  
843 Cambridge University Press.

844 Jackson, M. P., & Hudec, M. R. (2005). Stratigraphic record of translation down  
845 ramps in a passive-margin salt detachment. *Journal of Structural Geology*, 27(5),  
846 889-911.

847 Jackson, C. A. L., Jackson, M. P., & Hudec, M. R. (2015). Understanding the  
848 kinematics of salt-bearing passive margins: A critical test of competing hypotheses  
849 for the origin of the Albian Gap, Santos Basin, offshore Brazil. *Geological Society  
850 of America Bulletin*, 127(11-12), 1730-1751.

851 Jackson, C. A. L., Rodriguez, C. R., Rotevatn, A., & Bell, R. E. (2014). Geological  
852 and geophysical expression of a primary salt weld: An example from the Santos  
853 Basin, Brazil. *Interpretation*, 2(4), SM77-SM89.

854 Jackson, C. A. L., Jackson, M. P., Hudec, M. R., & Rodriguez, C. R. (2015).  
855 Enigmatic structures within salt walls of the Santos Basin—Part 1: Geometry and  
856 kinematics from 3D seismic reflection and well data. *Journal of Structural  
857 Geology*, 75, 135-162.

858 Jones, I. F., & Davison, I. (2014). Seismic imaging in and around salt  
859 bodies. *Interpretation*, 2(4), SL1-SL20.

860 Karner, G. D., & Gambôa, L. A. P. (2007). Timing and origin of the South Atlantic  
861 pre-salt sag basins and their capping evaporites. *Geological Society, London,  
862 Special Publications*, 285(1), 15-35.

863 Marton, G., Tari, G. & Lehmann, C. (1998) Evolution of salt-related structures and  
864 their impact on the post-salt petroleum systems of the Lower Congo Basin,

865 offshore Angola. *In*: American Association of Petroleum Geologists International  
866 Conference and Exhibition, Rio de Janeiro. Extended Abstracts Volume, 834–834.

867 Marton, G., Tari, G. & Lehmann, C. (2000). Evolution of the Angolan Passive  
868 Margin, West Africa, With Emphasis on Post-Salt Structural Styles. *Atlantic rifts*  
869 *and continental margins*, 129-149.

870 McClay, K. R. (1990). Extensional fault systems in sedimentary basins: a review of  
871 analogue model studies. *Marine and petroleum Geology*, 7(3), 206-233.

872 McClay, K. R., & Scott, A. D. (1991). Experimental models of hangingwall  
873 deformation in ramp-flat listric extensional fault systems. *Tectonophysics*, 188(1-2),  
874 85-96.

875 McClay, K. R. (1996). Recent advances in analogue modelling: uses in section  
876 interpretation and validation. *Geological Society, London, Special*  
877 *Publications*, 99(1), 201-225.

878 Meisling, K. E., Cobbold, P. R., & Mount, V. S. (2001). Segmentation of an  
879 obliquely rifted margin, Campos and Santos basins, southeastern Brazil. *AAPG*  
880 *bulletin*, 85(11), 1903-1924.

881 Modica, C. J., & Brush, E. R. (2004). Postrift sequence stratigraphy,  
882 paleogeography, and fill history of the deep-water Santos Basin, offshore  
883 southeast Brazil. *AAPG bulletin*, 88(7), 923-945.

884 Mohriak, W.U., Macedo, J.M., Castellani, R.T., Rangel, H.D., Barros, A.Z.N., Latgé,  
885 M.A.L., Mizusaki, A.M.P., Szatmari, P., Demercian, L.S., Rizzo, J.G. & Aires, J.R.

886 (1995). Salt tectonics and structural styles in the deep-water province of the Cabo  
887 Frio region, Rio de Janeiro, Brazil. *In: Jackson, M. P. A., Roberts, D. G., Snelson,*  
888 *S. (eds) Salt tectonics: a global perspective. AAPG Memoir 65, 273-304.*

889 Mohriak, W., Nemčok, M., & Enciso, G. (2008). South Atlantic divergent margin  
890 evolution: rift-border uplift and salt tectonics in the basins of SE Brazil. *Geological*  
891 *Society, London, Special Publications, 294(1), 365-398.*

892 Mohriak, W., Szatmari, P., & Anjos, S. M. C. (2009). Sal: Geologia e Tectônica;  
893 Exemplos nas Bacias Brasileiras. *Terrae Didatica, 4(1).*

894 Mohriak, W. U., Szatmari, P., & Anjos, S. (2012). Salt: geology and tectonics of  
895 selected Brazilian basins in their global context. *Geological Society, London,*  
896 *Special Publications, 363(1), 131-158.*

897 Mohriak, W. (2015). Pre-Salt Carbonate Reservoirs in the South Atlantic and  
898 World-wide Analogs. In AAPG Geosciences Technology Workshop “Carbonate  
899 Plays around the World-Analogues to Support Exploration and Development (pp.  
900 4-5).

901 Osmundsen, P. T., Bakke, B., Svendby, A. K., & Andersen, T. B. (2000).  
902 Architecture of the Middle Devonian Kvamshesten Group, western Norway:  
903 sedimentary response to deformation above a ramp-flat extensional  
904 fault. *Geological Society, London, Special Publications, 180(1), 503-535.*

905 Peel, F., Jackson, M.P. & Ormerod, D. (1998) Influence of Major Steps in the Base  
906 of Salt on the Structural Style of Overlying Thin-skinned Structures in Deep Water

907 Angola, American Association of Petroleum Geologists International Conference  
908 and Exhibition, Rio de Janeiro, Brazil, November, Extended Abstracts Volume, pp.  
909 366-367.

910 Quirk, D. G., Schødt, N., Lassen, B., Ings, S. J., Hsu, D., Hirsch, K. K., & Von  
911 Nicolai, C. (2012). Salt tectonics on passive margins: examples from Santos,  
912 Campos and Kwanza basins. *Geological Society, London, Special*  
913 *Publications*, 363(1), 207-244.

914 Peel, F. J. (2014). The engines of gravity-driven movement on passive margins:  
915 Quantifying the relative contribution of spreading vs. gravity sliding  
916 mechanisms. *Tectonophysics*, 633, 126-142.

917 Rowan, M. G., Jackson, M. P., & Trudgill, B. D. (1999). Salt-related fault families  
918 and fault welds in the northern Gulf of Mexico. *AAPG bulletin*, 83(9), 1454-1484.

919 Rowan, M. G., Peel, F. J., & Vendeville, B. C. (2004). Gravity-driven fold belts on  
920 passive margins.

921 Rowan, M. G., 2004, Do salt welds seal?: Presented at GCSSEPM Foundation  
922 24th Annual Bob F. Perkins Research Conference, 390–403.

923 Rowan, M.G., 2014. Passive-margin salt basins: hyperextension, evaporite  
924 deposition, and salt tectonics. *Basin Research*, 26(1), 154-182.

925 Sanchis, E. & Séranne, M. (2000). Structural style and tectonic evolution of a  
926 polyphase extensional basin of the Gulf of Lion passive margin: the Tertiary Ales  
927 basin, southern France. *Tectonophysics*, 322(3), 219-242.

928 Schuster, D. C. (1995). Deformation of allochthonous salt and evolution of related  
929 salt-structural systems, eastern Louisiana Gulf Coast. *In: Jackson, M. P. A.,*  
930 *Roberts, D. G., Snelson, S. (eds) Salt tectonics: a global perspective. AAPG*  
931 *Memoir 65, 177-198.*

932 Tari, G., & Jabour, H. (2013). Salt tectonics along the Atlantic margin of  
933 Morocco. *Geological Society, London, Special Publications, 369(1), 337-353.*

934 Weijermars, R., Jackson, M. T., & Vendeville, B. (1993). Rheological and tectonic  
935 modeling of salt provinces. *Tectonophysics, 217(1-2), 143-174.*

936



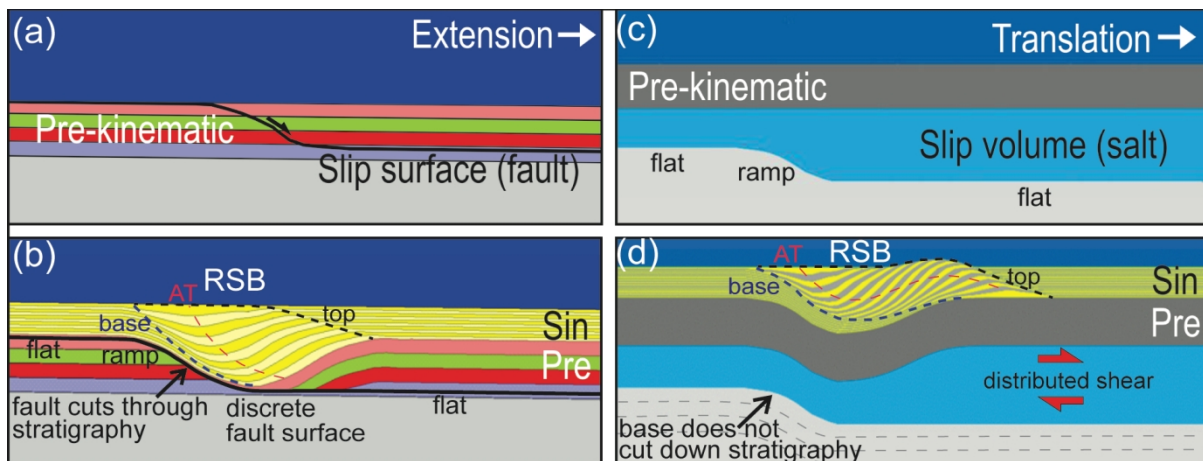


Figure 1: Models of RSB development. (a-b) represent "classic" RSBs, with (a) illustrating the system prior to deformation, and (b), the system during extension with development of a RSB characterized by an asymmetric depocentre with basinward-dipping axial trace (AT) above a discrete extensional fault that cuts down through stratigraphy in a ramp-flat trajectory. Movement of the hanging-wall creates differential amounts of subsidence and as long as the fault is extensional, there is no hanging-wall uplift. This contrasts with the model for salt-detached RSBs shown in (c-d). The system is not extensional; instead it the RSB forms by translation of the cover over a viscous salt layer. A downward offset of the base of salt takes the place of the fault ramp. The offset may not cut down through stratigraphy. Shear strain is distributed through the viscous salt and results in uplift on the downdip side of salt-detached RSBs. The base and top boundaries of the RSBs are diachronous, and consist either of onlap/offlap unconformity surfaces, or regions of abrupt stratal thinning.

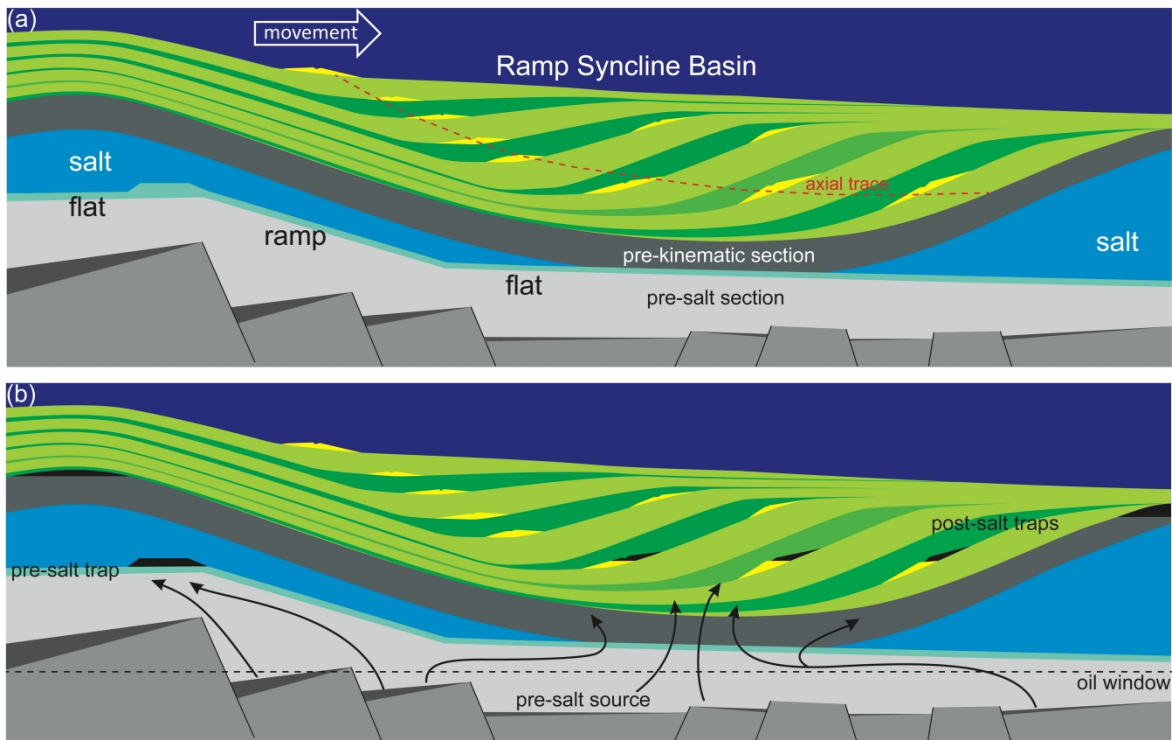


Figure 2: Schematic cross-sections: (a) illustrating typical geometry of RSBs formed above salt-detachments with a basinward-dipping ramp; and (b) displaying potential hydrocarbon plays that can be associated with RSBs in these settings: pre-salt carbonates (blueish green) occurring at the top of the pre-salt ramps and below the updip limit of the RSBs (e.g. Tupi and Iracema discoveries); carbonates on the crest of salt anticlines, and supra-salt sandier intervals juxtaposed above deeper and mature pre-salt source rocks, which can be charged with salt welding below the RSB.

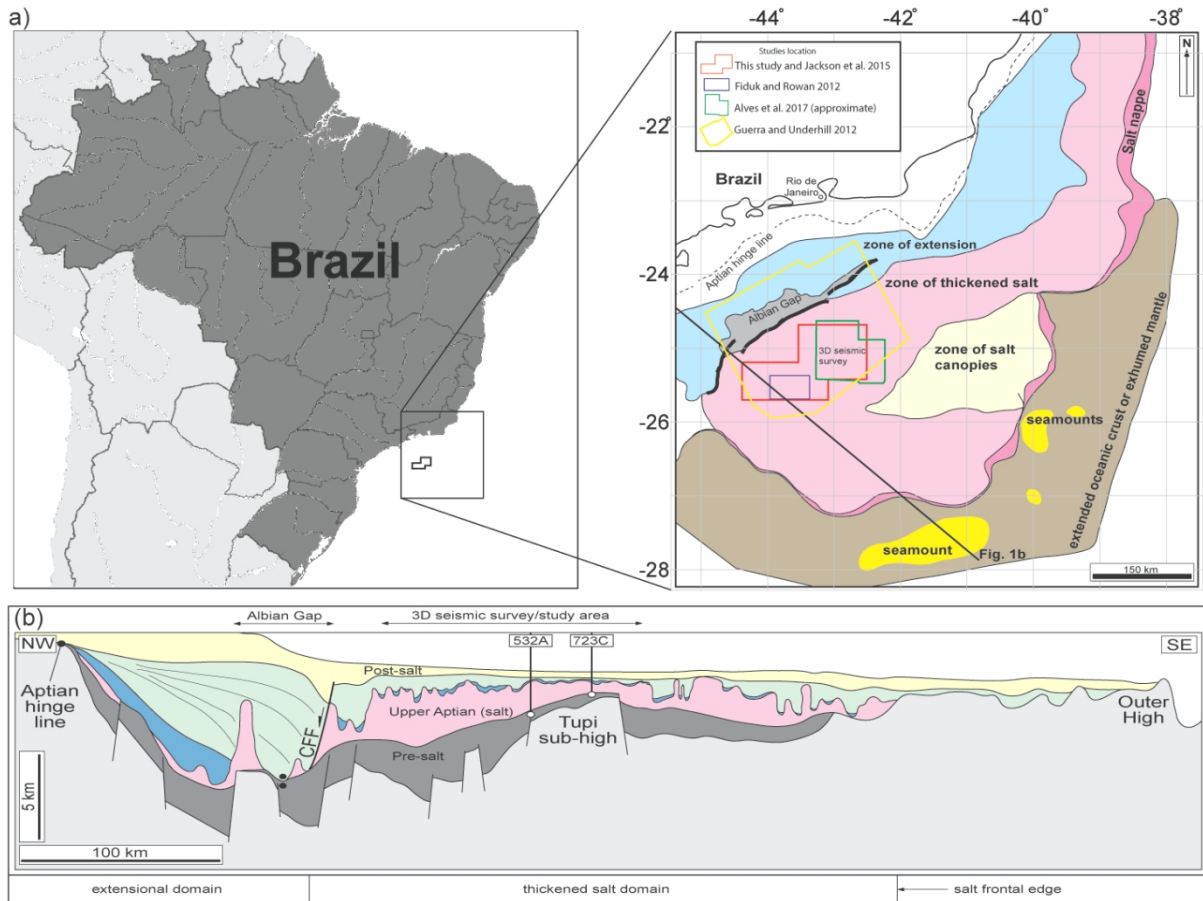


Figure 3: (a) Location map showing the 3D dataset and study area (Jackson et al. 2015) in its regional context. (b) Simplified geoseismic section across the central Santos Basin illustrating basement structures and salt-related structural provinces. Location of section is shown in (a).

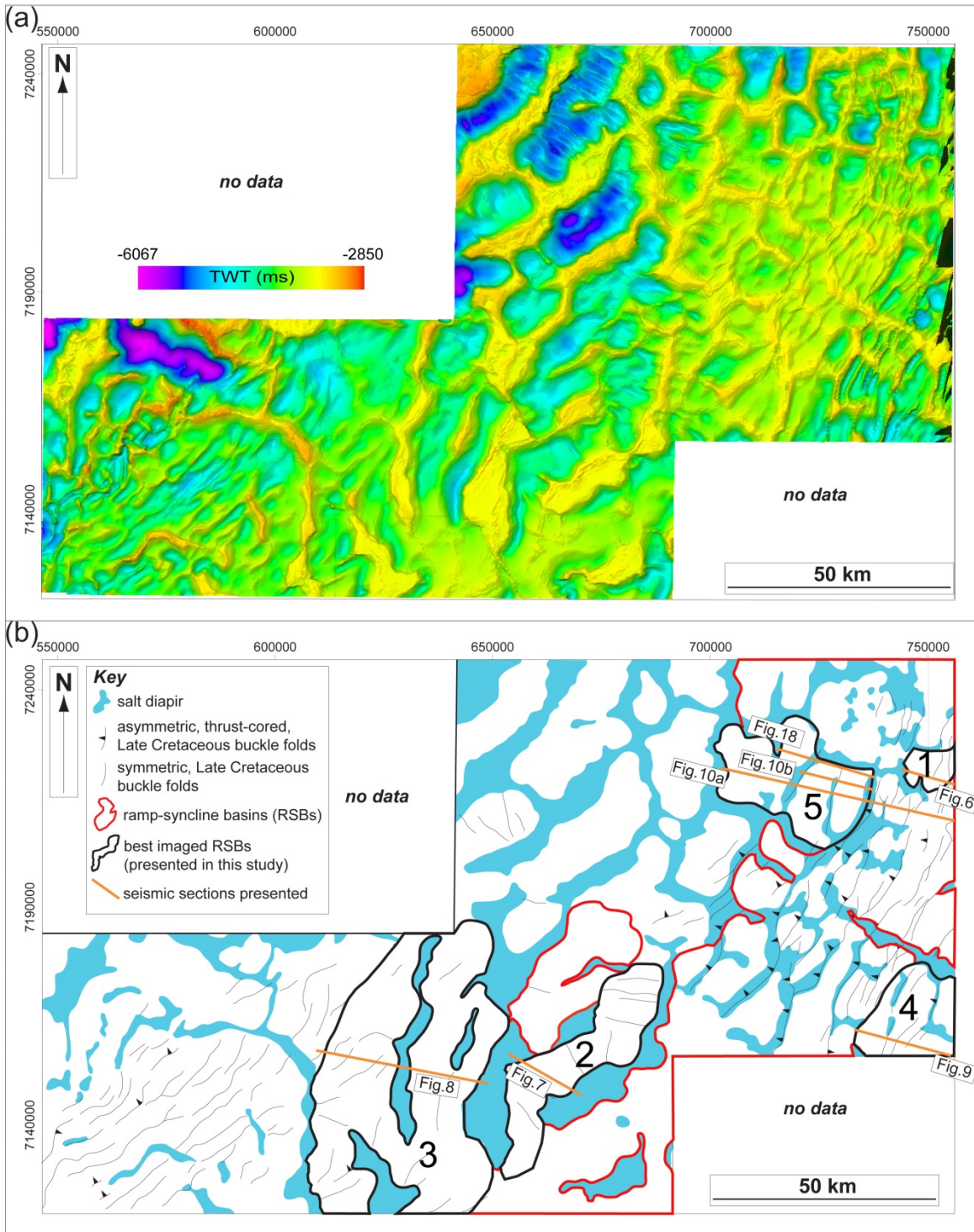


Figure 4: (a) Top-salt map showing complex pattern of salt walls and stocks. (b) Drawn top-salt map with main structures (adapted from Jackson et al. 2015), and distribution of RSBs. The examples presented in this study are in black polygons (RSB 1-5).



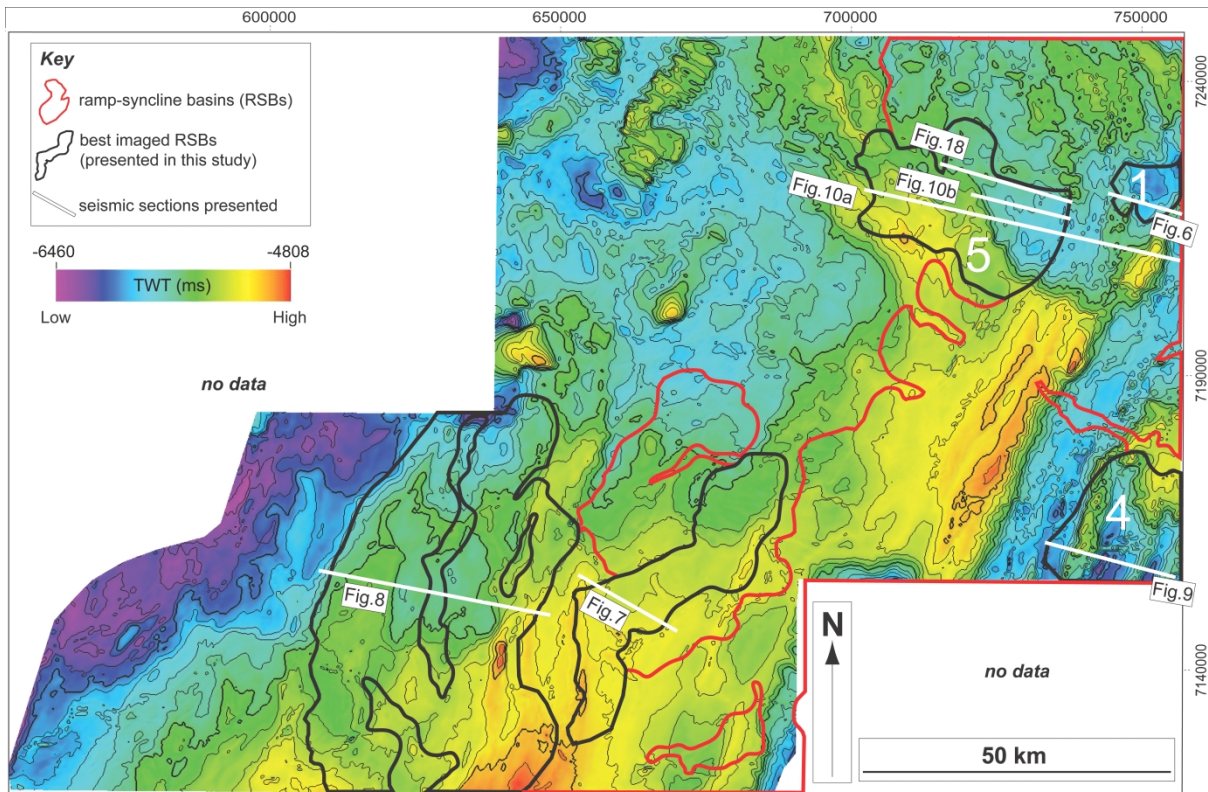
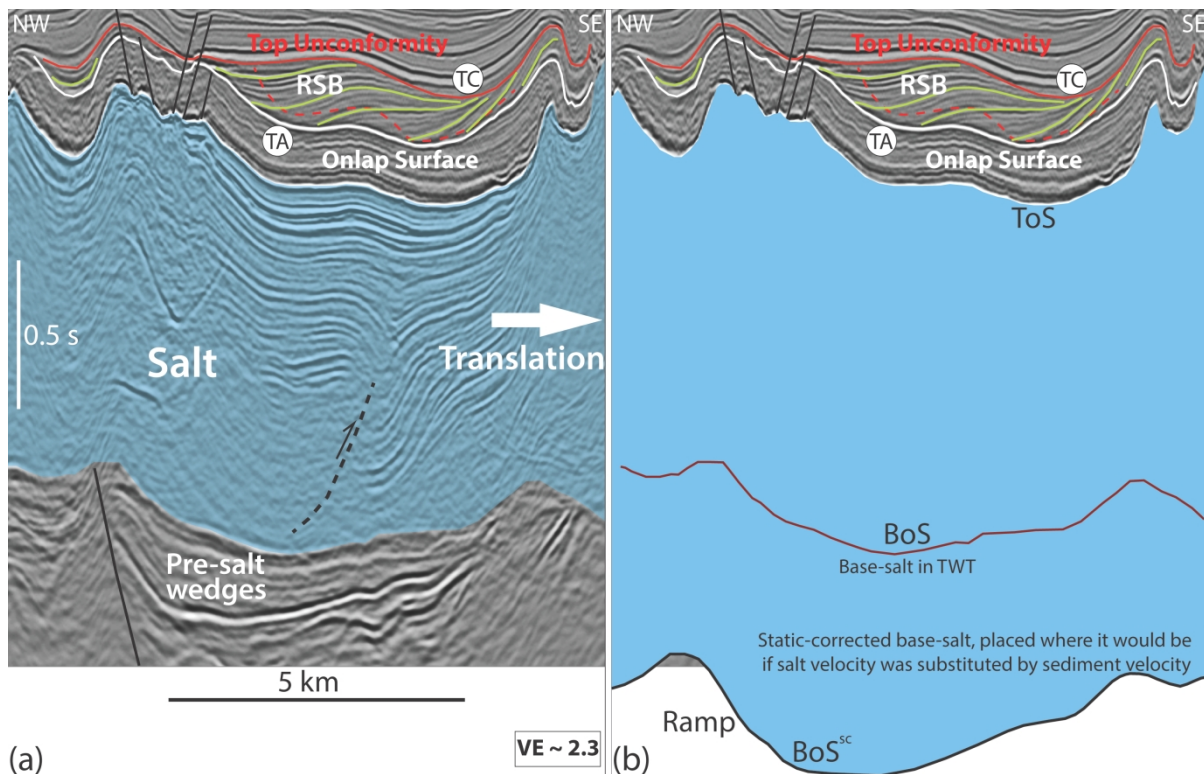


Figure 5: Static-corrected base-salt map showing the largest base-salt structures in the area. They trend NNE to NE, although the northernmost high (beneath RSB 5) trends NNW. Map shows that RSBs (red and black polygons) are distributed above and/or basinward of the main base-salt steps.



(a) Interpreted seismic section of RSB 1 with salt in blue and faults in black. Top Albian (TA) and top Cretaceous (TC) horizons based on Jackson et al. 2015. RSB characterized by landward-dipping and thickening sigmoidal strata (green) above an onlap surface (white, top Albian) and capped by a diachronous unconformity (red) that finishes updip at top Cretaceous. RSB axial trace (dashed red) steepens landward. Intra-salt seaward-vergent shear zones (black dashed lines) indicate lateral movement. Pre-salt wedges and faults are used as a cross-check of the static-corrected base-salt map and base-salt structures. In (b), the relationship between the RSB and base-salt structure is presented through the static-corrected base-salt (BoS<sup>sc</sup>) which shows that the RSB landward edge occurs above the top of a base-salt basinward-dipping ramp.



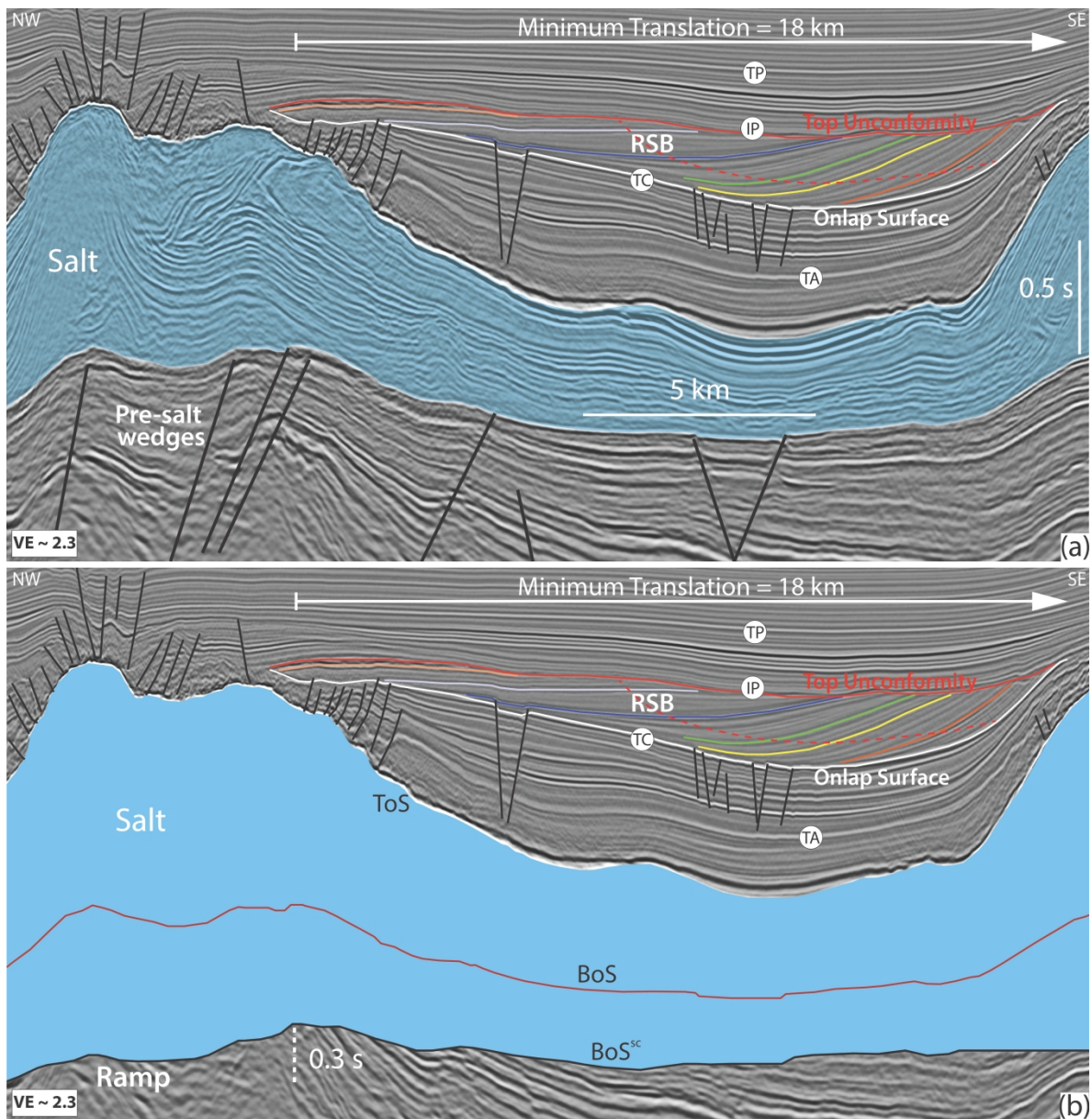


Figure 7: Seismic sections of the landward segment of RSB 2. Key horizons based on Jackson et al. 2015 are presented: top Albian (TA), top Cretaceous (TC), intra-Paleocene unconformity (IP) and top Paleocene (TP). In (a), interpretation of RSB 2, characterized by a well-defined onlap surface (white, TC) being onlapped by landward-dipping and thickening strata (colored lines), defined by a landward-steepening axial-trace (dashed red) and capped by the intra-Paleocene unconformity (red). Faults are in black. Pre-salt wedges and faults are used as a cross-check of static-corrected base-salt map and base-salt structures. In (b), the RSB is presented in the context of the static-corrected base-salt (BoS<sup>sc</sup>) to illustrate that the RSB finishes updip above a base-salt landward-dipping ramp, being surrounded by diapirs. Minimum translation of 18 km is measured from first landward onlap point within the RSB to the top of the ramp.

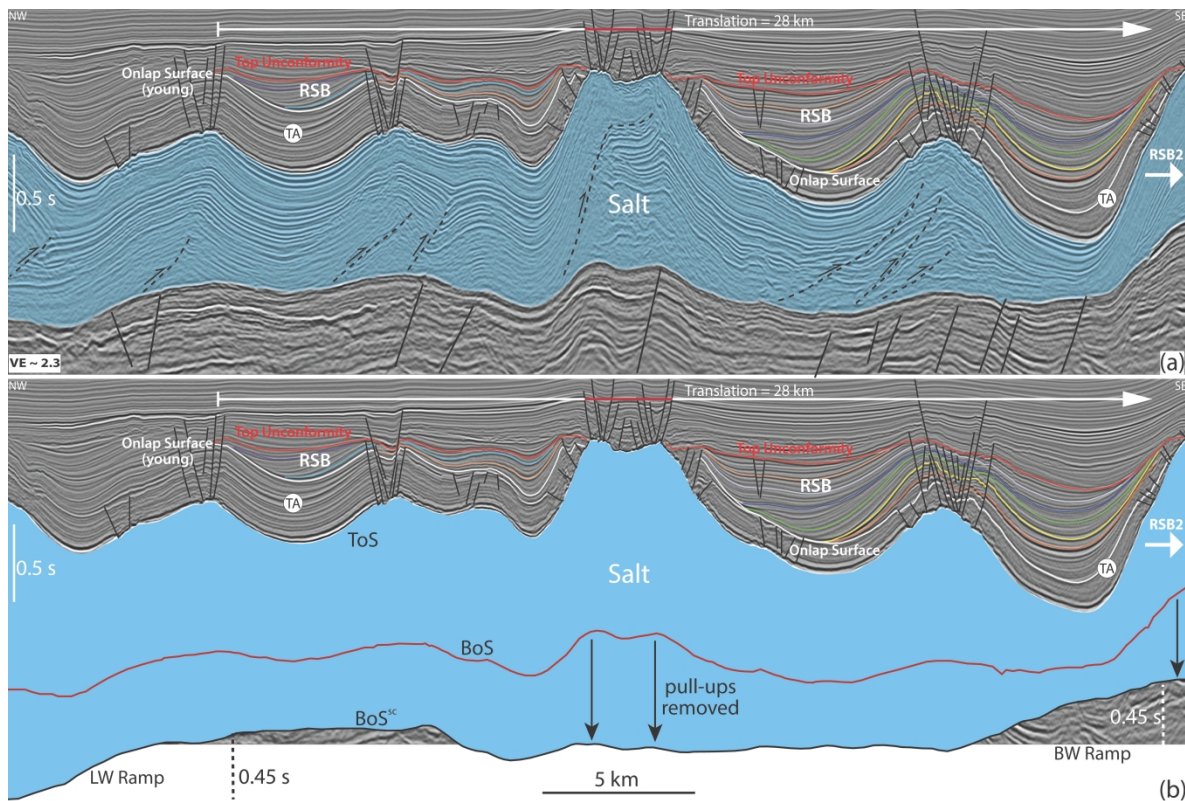


Figure 8: (a) Interpreted seismic section of the entire RSB 3 system showing a total of 28 km of translation. In (b), RSB is displayed in combination with the static-corrected base-salt (BoS<sup>sc</sup>) to demonstrate its relationship with base-salt topography and how this approach eliminates velocity artefacts due to high velocities of the salt interval. The RSB is characterized by a well-defined and diachronous onlap surface (white) being onlapped by landward-dipping and thickening strata (colored lines) and truncated at the top by a diachronous unconformity (red). The basal onlap surface starts at the top Albian (TA) horizon and becomes progressively younger landward. RSB 3 is limited updip by a salt anticline formed above a landward-dipping base-salt ramp, and downdip by a large salt wall that also limits RSB 2 basinward. RSB 3 is segmented and folded by syn- to late diapirism. Faults are in black and pre-salt faults are used as a cross-check of base-salt structures. Intra-salt shear zones (black dashed lines) indicate lateral movement.



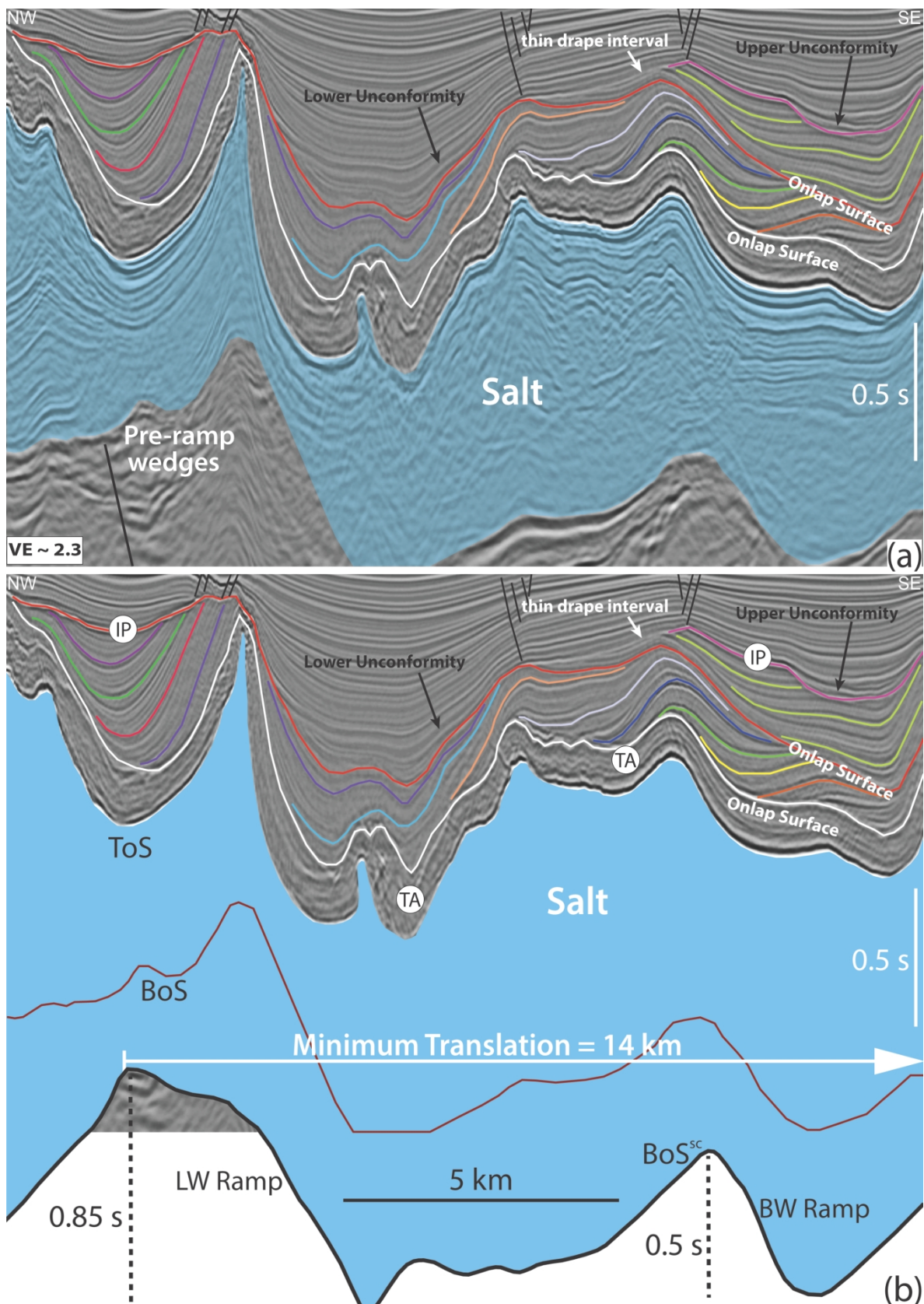


Figure 9: (a) Interpreted section of RSB 4 showing stacked RSBs and onlap surfaces (white and red). In (b) the stacked RSBs are show in the context of static-corrected base-salt (BoS<sup>sc</sup>) and key horizons are presented: top Albian (TA), and intra-Paleocene unconformity (IP). Salt is in blue, faults in black and intra-RSB horizons in coloured lines. Onlap surfaces and top unconformity get slightly younger landward. Top unconformity of lower RSB corresponds to the onlap surface of upper RSB (red) until

becoming separated landward by a thin drape interval that is deposited updip of the basinward (BW) base-salt ramp and RSB. This surface (red) is aged mid-Cretaceous basinward and Intra-Paleocene landward evidencing its diachroneity. Only a minimum translation estimate of 14 km is obtained because RSB 5 is located at the edge of the data and is not visualized entirely.



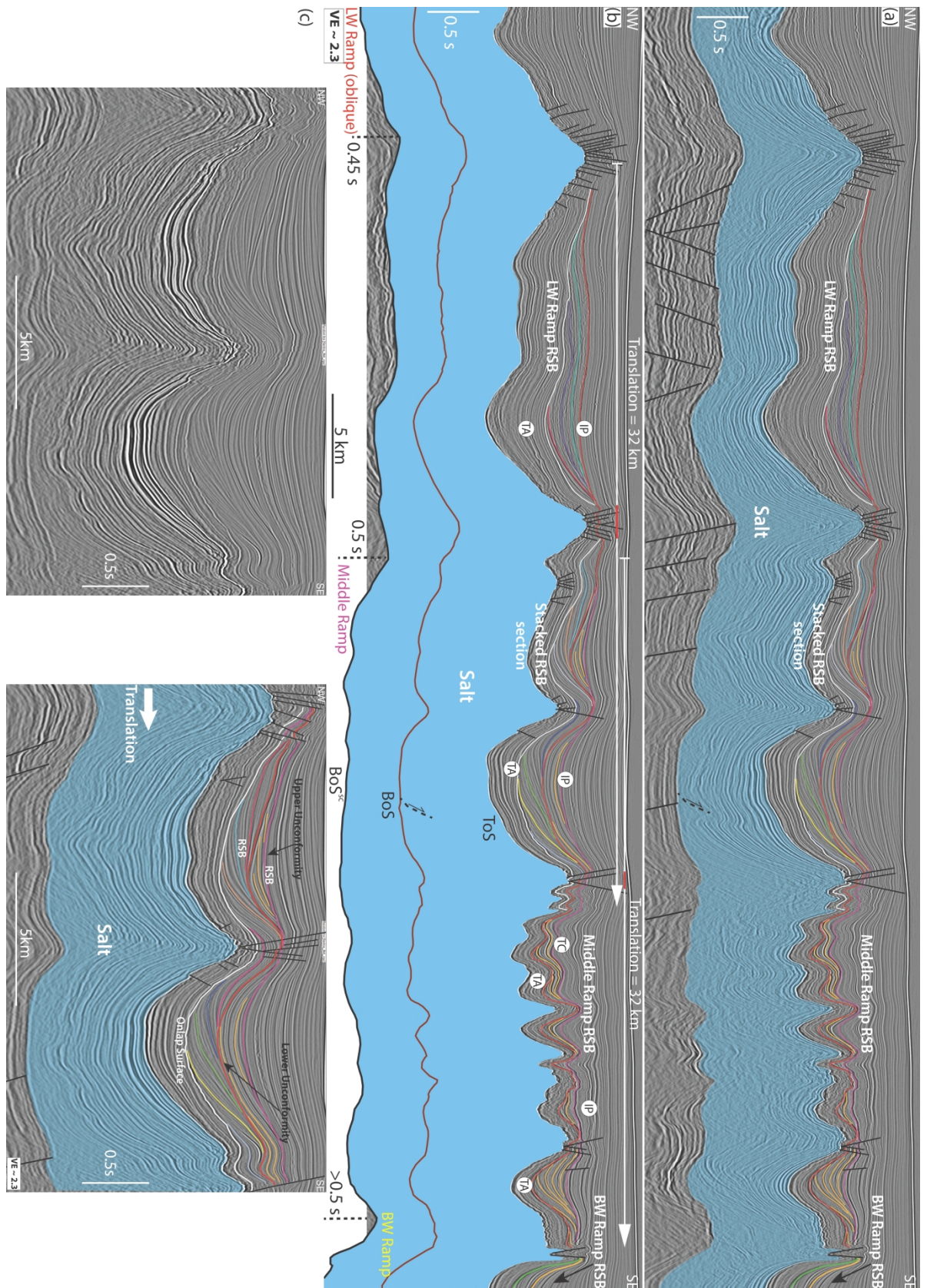


Figure 10: (a-b) Regional seismic sections of RSB 5 showing stacked RSBs and onlap surfaces (white and red lines) in the middle of the section. Salt is in blue and faults in black. In (b), the static-corrected base-salt (BoS<sup>sc</sup>) and key horizons, top Albian (TA), top Cretaceous (TC) and intra-Paleocene unconformity (IP) are presented. Three RSBs are shown: The basinwardmost one is

formed above a basinward-dipping ramp but appears only at the edge of the data. The middle RSB is formed by translation above a basinward-dipping ramp (middle ramp) and its landward portion is stacked on top of the basinward portion of the third, landward RSB, which is formed above a landward-dipping ramp. These RSBs are strongly affected by synchronous diapirism, folding and faulting but still show the typical geometries of RSB systems with sigmoidal landward-dipping and expanding strata. In (c), uninterpreted and interpreted localized sections of RSB 5, showing a zoom of the stacked RSBs section. A total of 32 km of translation is estimated for each of the stacked RSBs. The fact that both RSBs record the same amount of translation can be used as a cross-check for this measure.



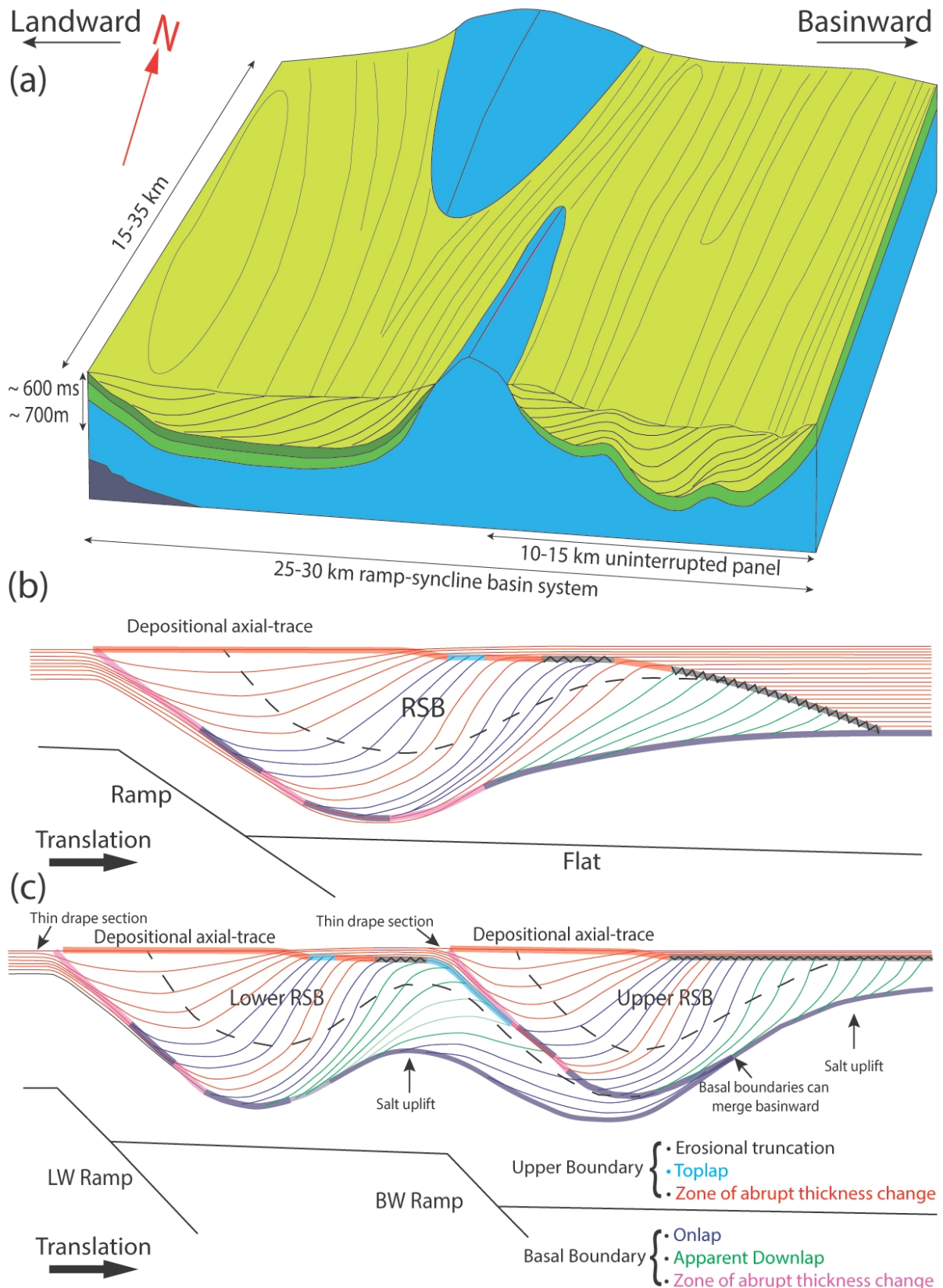
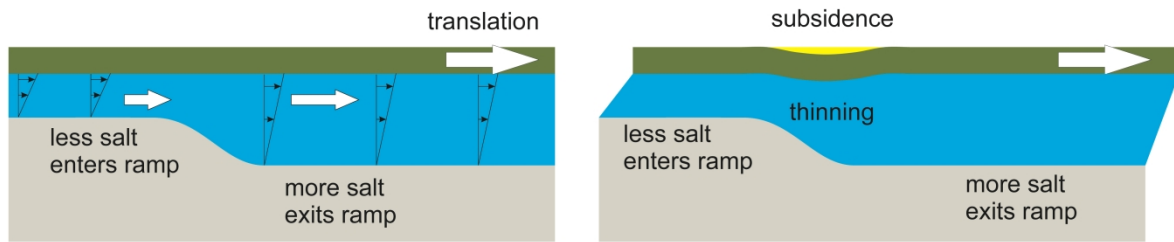


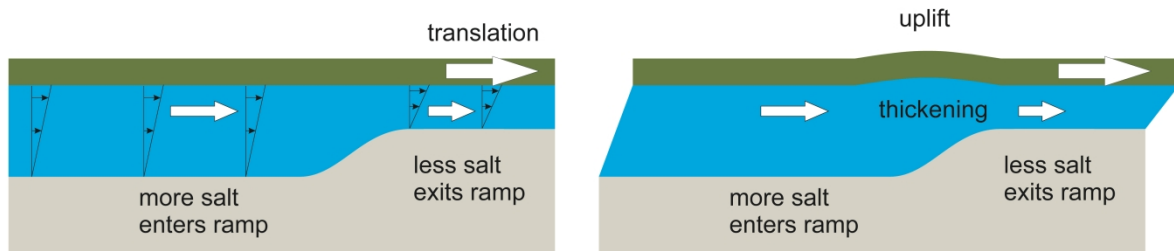
Figure 11: (a) Schematic 3D diagram of RSBs geometries, dimensions and relationship with diapirs and base-salt steps. (b) Summary of the 2D stratigraphic architecture showing the typical variations of strata termination of RSBs in the Santos Basin. The basal surface has terminations ranging from: i) abrupt apparent downlap at basinward edge, ii) abrupt onlap and iii) transition from thicker and

steeper section within the RSB to a thin draping interval at its landward edge. The top unconformity has a similar pattern of terminations ranging from abrupt erosional and toplap terminations downdip, to more transitional strata geometries updip. In (c), summary of the 2D stratigraphic architecture and strata terminations of stacked RSBs. The lower RSB finishes landward above the top of the landward ramp and the upper RSB finishes above the top of the basinward ramp. Stratal termination is similar to simple RSBs, but the lower RSB top unconformity acts as the onlap surface of the upper RSB along most of its length. A thin drape section can separate these surfaces at the upper RSB landward edge.

(a) Subsidence due to change in salt thickness with time (downramp)



(b) uplift due to change in salt thickness with time (upramp)



(c) subsidence/uplift due to dip of the top salt surface

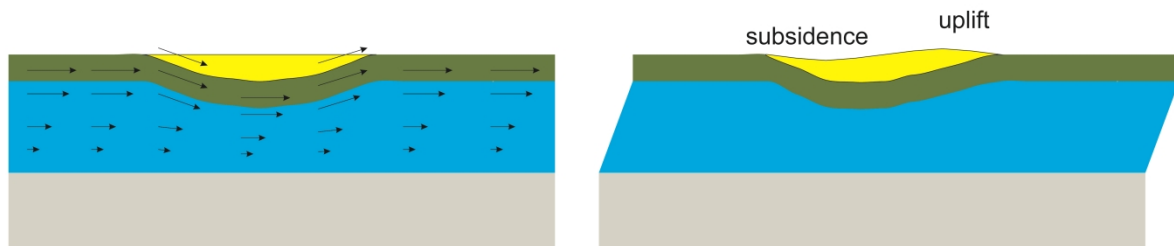


Figure 12: Conceptual 2D diagrams of the dynamics of Couette salt flow and variation of total salt-flux over a base-salt (a) basinward-dipping ramp and (b) landward-dipping ramp. In (a) the amount of salt leaving the ramp is lesser than the amount of salt arriving at the top of the ramp generating thinning of the salt layer, subsidence of the cover and generation of a depocentre immediately above the ramp. In (b), the amount of salt leaving the ramp is less than the amount of salt arriving, which results in salt thickening and uplift of the cover above the ramp. In (c), the diagram illustrates the effect of topography generated by translation above base-salt ramps by downward movement of the cover where the top-salt dips basinward and upward movement of the cover where the top-salt interval dips landward generating areas of local subsidence updip and uplift downdip.

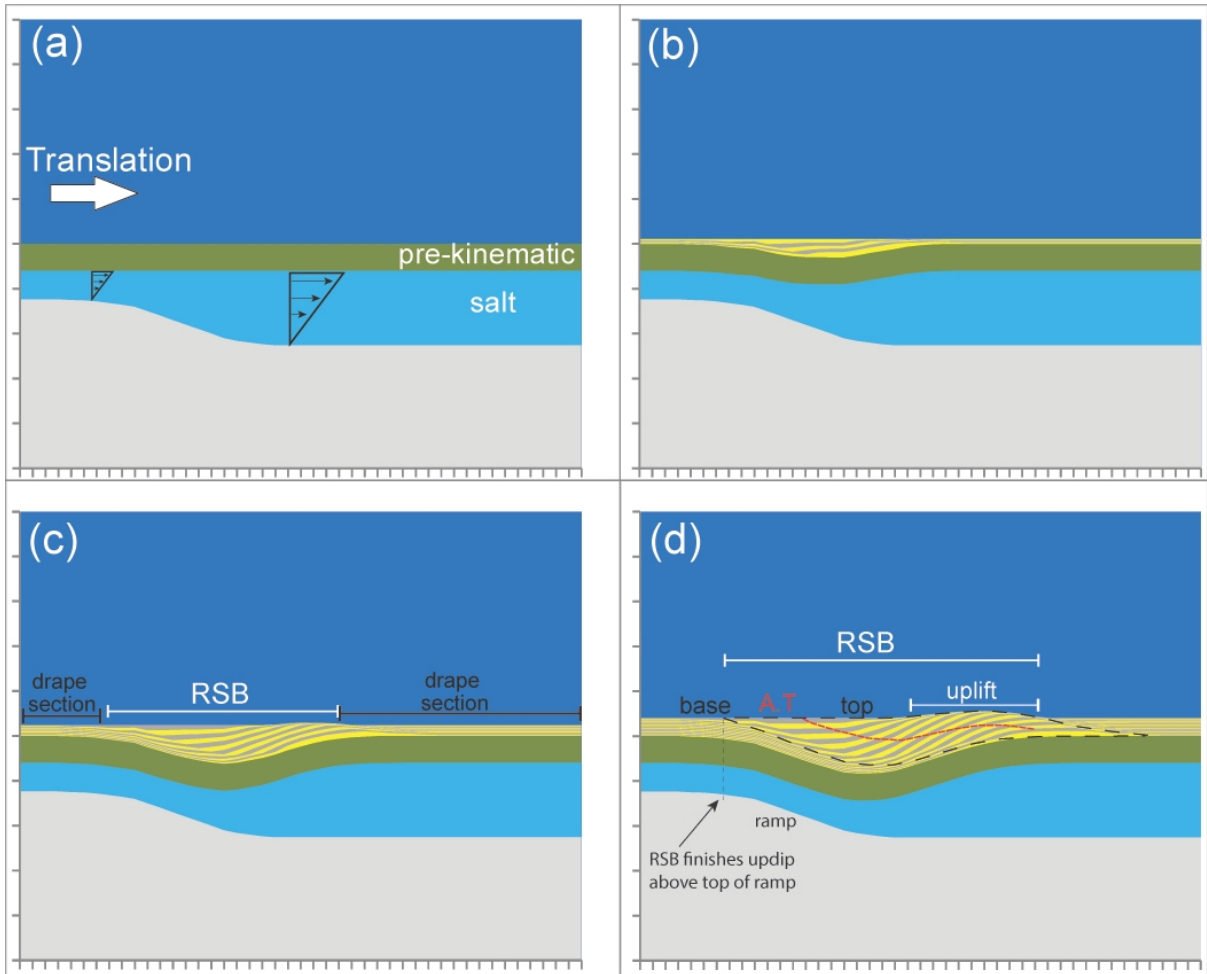


Figure 13: Numerical model simulating planar Couette flow and salt drag with overburden translation above a salt layer with a basal basinward-dipping ramp, which results in the development of a RSB above the ramp. Sequential evolution presented from (a) to (d). Syn-kinematic sediments are represented by yellow and grey layers.



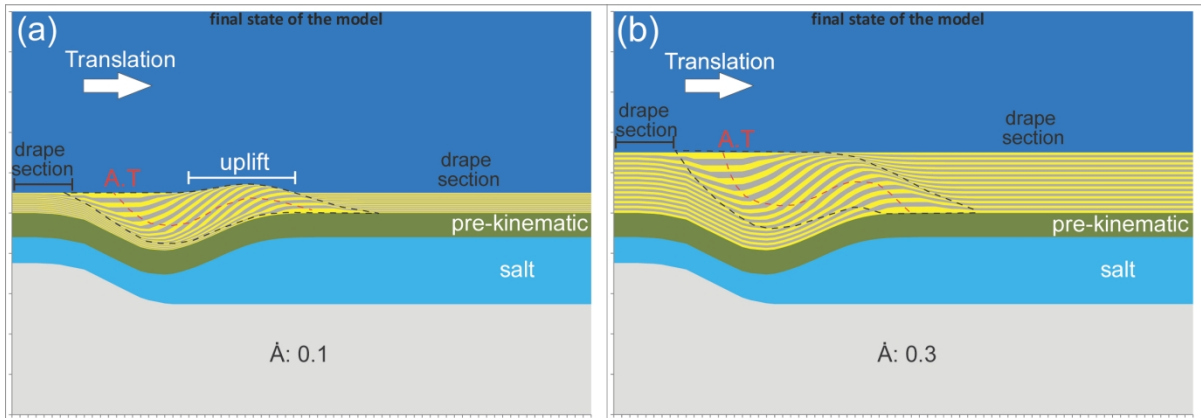


Figure 14: Final state of models simulating cover translation above a salt detachment with a base-salt ramp illustrating how variations of aggradation rate ( $\dot{A}$ ) can produce different stratigraphic architectures and stratal termination patterns. ( $\dot{A}$ ) in these models is non-dimensional so their variations are purely relative to translation rates ( $\dot{v}$ ). In (a) aggradation rate is 0.1 and the RSB is characterized by well-defined boundaries and uplift above the regional datum on the downdip side of the RSB. In (b) aggradation rate is 0.3 and the RSB is less asymmetric with upper and lower boundaries defined by a transition from thin section at regional dip to thicker and steeper section within the RSB. Translation rate ( $\dot{v}$ ) is the same in both models.

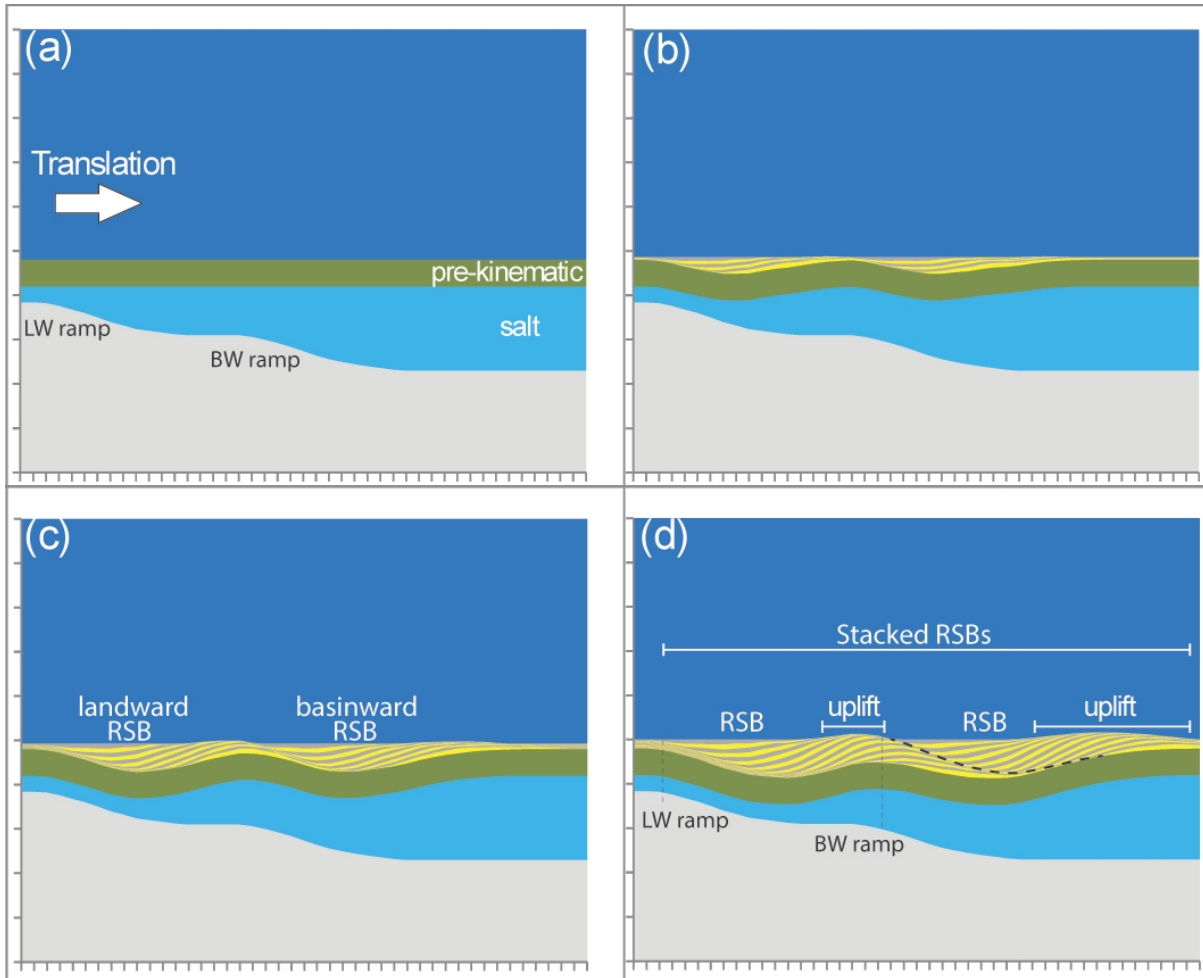


Figure 15: Numerical model simulating cover translation above a thick salt layer with 2 closely-spaced basinward-dipping ramps showing the sequential evolution of 2 stacked RSBs (a-d). The lower, landward RSB forms above the landward ramp while the upper, basinward RSB forms above the basinward ramp. Each of the RSBs finishes landward above their respective ramps. The top unconformity of the lower RSB acts as the onlap surface of the upper RSB (black dashed line). The upper and lower basal boundaries merge basinward while both top unconformities merge landward.

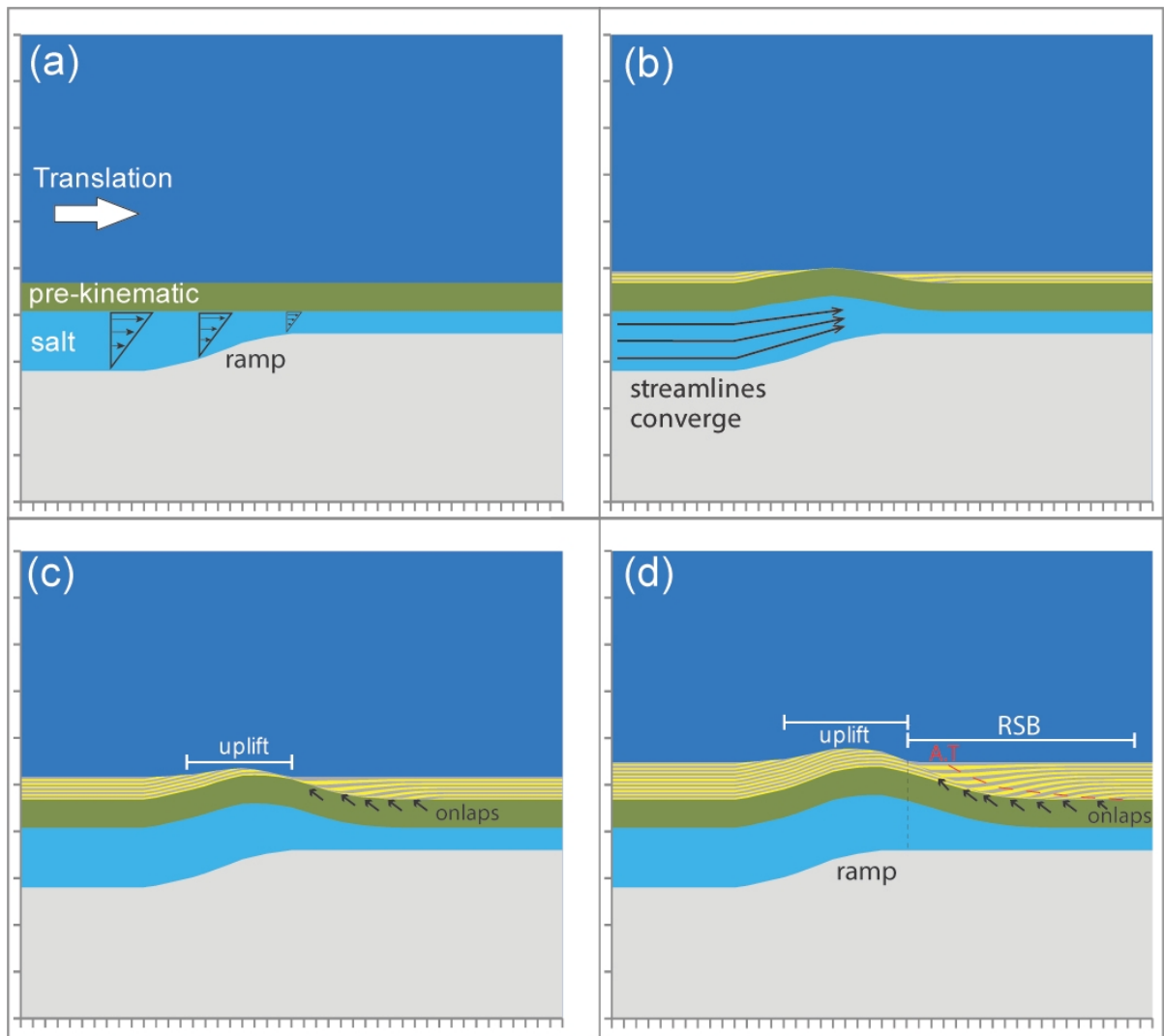


Figure 16: Numerical model simulating overburden translation and Couette salt flow above a landward-dipping base-salt ramp. Variations of salt flux across the step result in salt thickening over the ramp and development of a RSB basinward of it, above a base-salt flat. Sequential evolution is shown from (a) to (d).

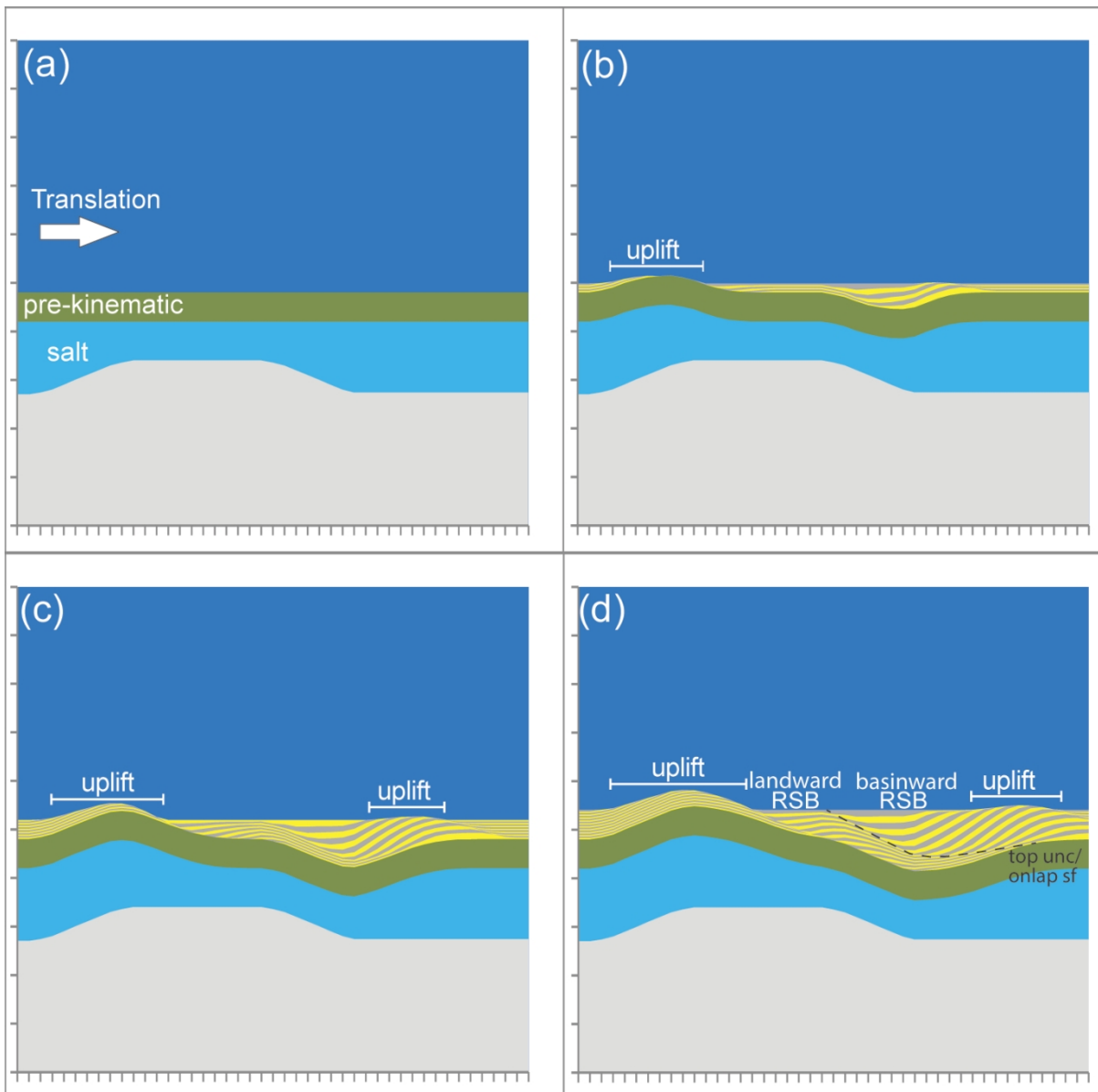


Figure 17: Numerical model showing the sequential evolution (a) to (d) of overburden translation and Couette-type salt flow above two oppositely dipping base-salt ramps and the development of hybrid stacked RSBs.

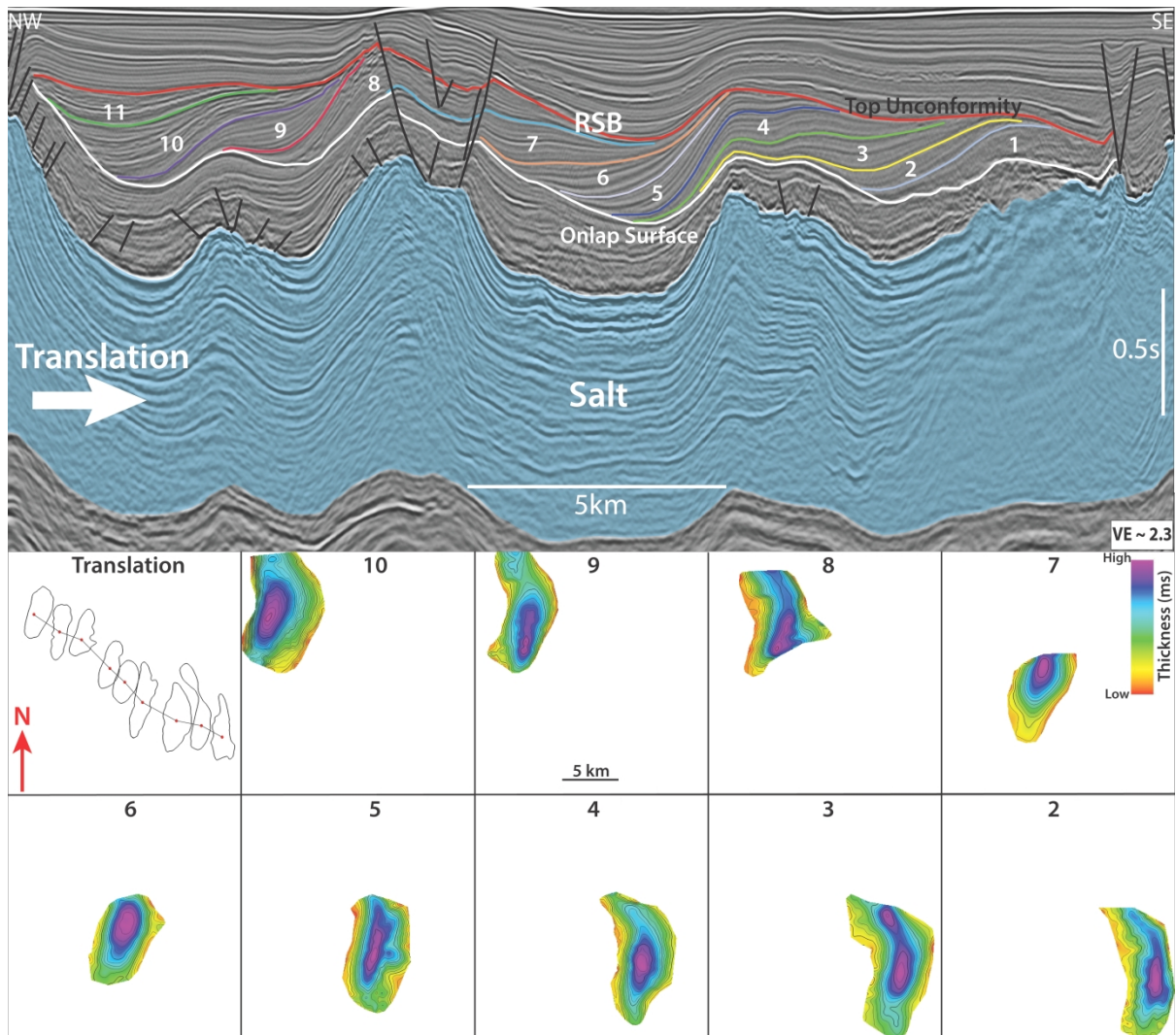
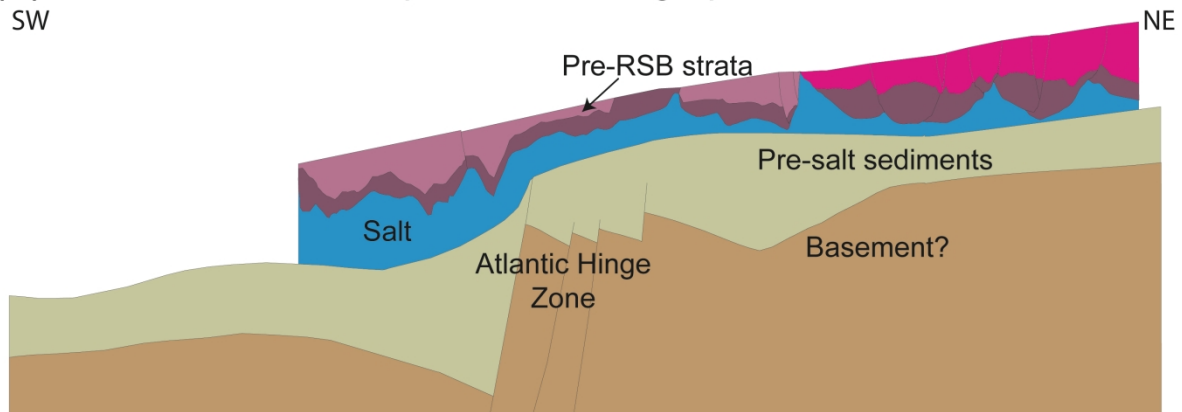
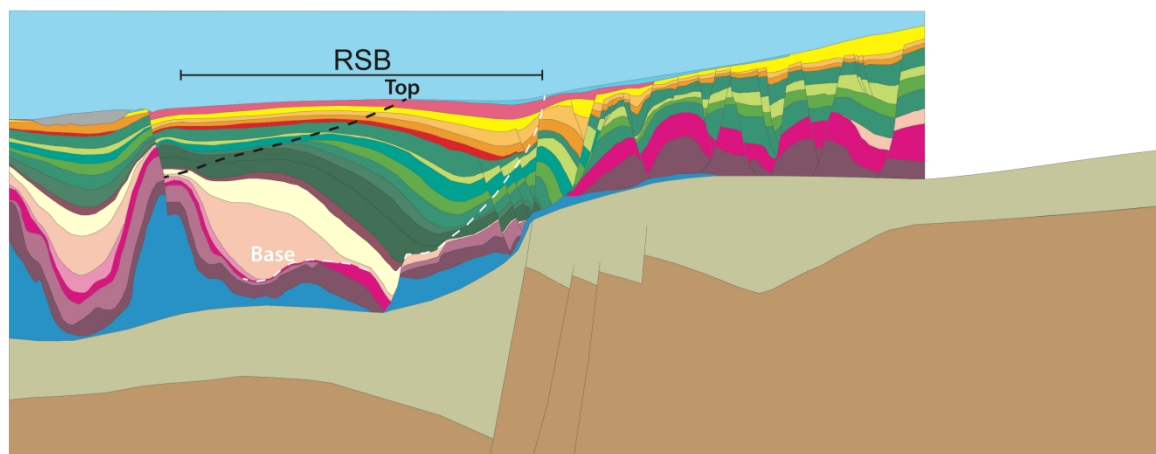


Figure 18: Interpreted seismic section of RSB 5 showing typical landward-dipping sigmoidal intervals and respective thickness maps illustrating the 3D kinematics of the system with 26.9 km of translation towards SE ( $120 \pm 15$  azimuth). Oldest intervals are located further downdip of the associated base-salt ramp. Thickness maps of intervals 1 and 11 are not shown because these intervals are affected by a higher degree of salt-related folding and faulting, which hinders the generation of confident maps.

(a) Restored and decompacted to stratigraphic horizon "x",  $v=5h$   
SW NE



(b) Present day depth structure,  $v=5h$



(c) Present day depth structure,  $v=h$

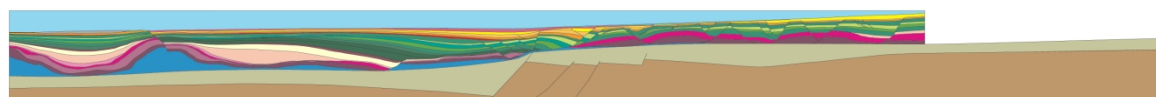


Figure 19: restoration of Line 214 from the Lower Kwanza Basin (adapted from Peel, 2014). Salt is in blue and RSB intervals are represented by colours ranging from purple, green, orange and yellow. RSB forms by translation over the Atlantic Hinge zone, which corresponds to a major basinward-dipping base-salt step. Original salt thickness varies from 1 km above the ramp to 2 km downdip. Translation is ongoing as the system is capped landward by the sea-floor. A total of 24 km of translation has been measured in this section.



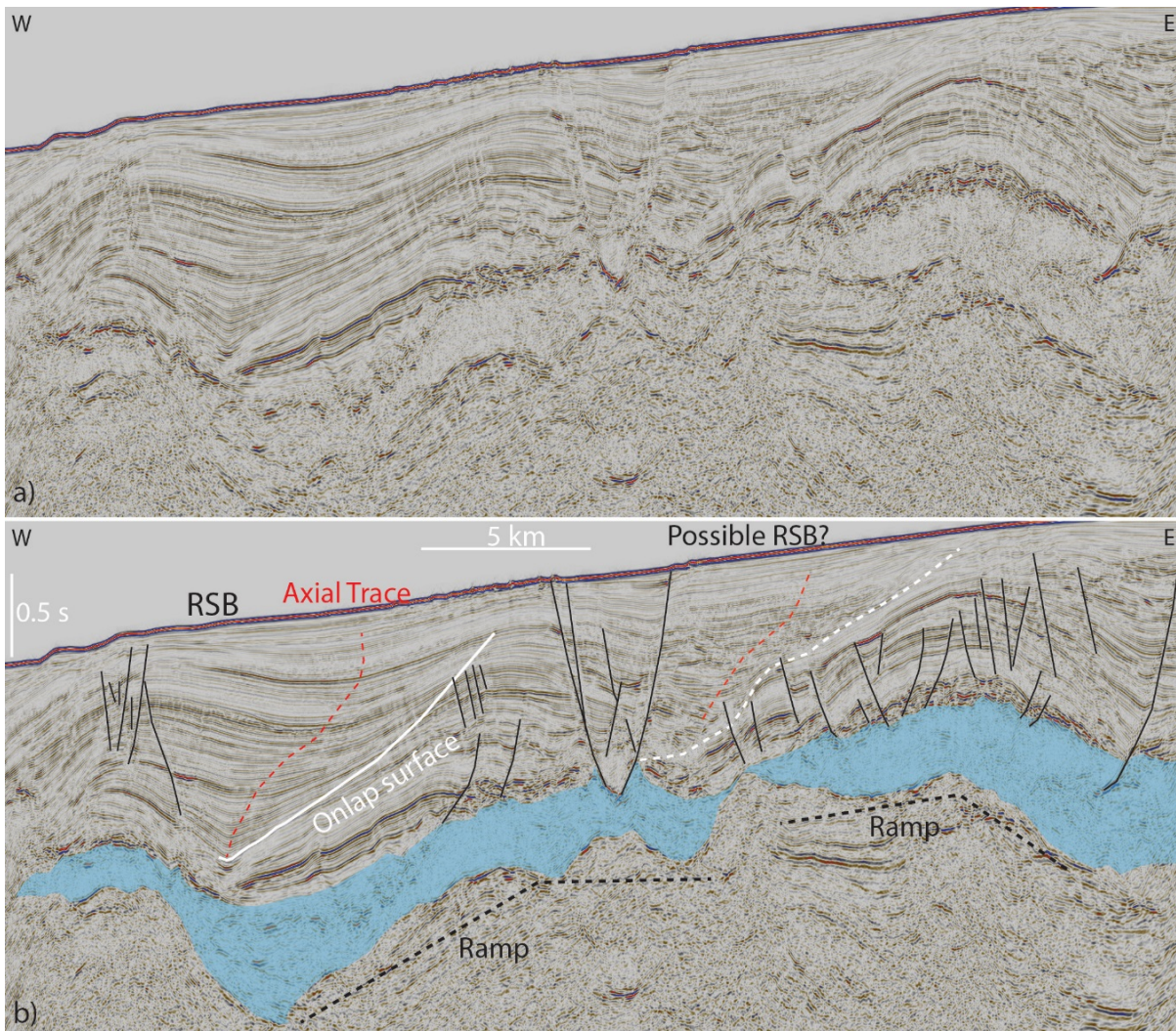


Figure 20: Seismic section showing a simple RSB formed above allochthonous salt (blue) with a base-salt basinward-dipping ramp in the Essaouira-Agadir Basin, Morocco. Another possible candidate of RSB appears to the East but the limited seismic resolution in the area hinders its clear identification.